De novo mutation and identity-by-descent drive disease haplotypes, biallelic traits and multilocus pathogenic variation

Zeynep Coban-Akdemir [1,2†], Xiaofei Song[1†], Francisco C. Ceballos[3†], Davut Pehlivan[1,4], Ender Karaca[1], Yavuz Bayram[1], Tadahiro Mitani[1], Tomasz Gambin[5], Shalini N. Jhangiani[6], Donna M. Muzny[6], Richard A. Lewis[1,7], Baylor Hopkins Center for Mendelian Genomics, Pengfei Liu[1], Eric Boerwinkle[2,6], Ada Hamosh[8], Richard A. Gibbs[1,6], V. Reid Sutton[1,9], Nara Sobreira[8], Claudia M. B. Carvalho[1,10], Chad A. Shaw[1,11,] Jennifer E. Posey[1], David Valle[8], James R. Lupski[1,6,7,9*]

1. Department of Molecular and Human Genetics, Baylor College of Medicine, Houston, TX 77030, USA

2. Human Genetics Center, Department of Epidemiology, Human Genetics, and Environmental Sciences, School of Public Health, The University of Texas Health Science Center at Houston, Houston, Texas, USA

3. Instituto de Salud Carlos III, National Center of Microbiology, Madrid, Spain

4. Section of Neurology, Department of Pediatrics, Baylor College of Medicine, Houston, TX 77030, USA

5. Institute of Computer Science, Warsaw University of Technology, Warsaw 00-665, Poland

6. Human Genome Sequencing Center, Baylor College of Medicine, Houston, TX 77030, USA

7. Department of Pediatrics, Baylor College of Medicine, Houston, TX 77030, USA

8. McKusick-Nathans Department of Genetic Medicine, Johns Hopkins University School of Medicine, Baltimore, MD 21205, USA

9. Texas Children's Hospital, Houston, TX 77030, USA

10. Pacific Northwest Research Institute, 720 Broadway Seattle, WA, 98122

11. Baylor Genetics, Houston, TX 77021, USA

[*] Correspondence: jlupski@bcm.edu

[†] These three authors contributed equally

Whereas new mutational events have been demonstrated to have a substantial impact on expressing rare disease traits in dominantly inherited Mendelian conditions, the relevance of the Clan Genomics hypothesis and new mutation has not been extensively tested in populations with a high frequency of recessive disease. We describe a cohort of 1,416 unrelated Turkish individuals and characterize population-based substructure and variation within this group. We investigate the occurrence and size of runs of homozygosity (ROH) within this cohort, and demonstrate an enrichment of ultra-rare, disease-causing variants within long-sized ROH. These findings support the role of new mutation in recessive disease: population substructure drives rapid generation of disease haplotypes that are shaped by recombination and characterized by new mutation. That such haplotypes are even more rare than their constituent alleles builds upon the Clan Genomics hypothesis that posits a role for new mutation – and newly configured haplotypes – in Mendelian disease.

Introduction

Population genetics has for many decades been applied as a means to uncover genetic variants that contribute to human disease, through the analysis of single nucleotide polymorphisms (SNPs). These SNPs are common to, and frequently shared among, geographically distinct populations, but enable a fine-scale mapping of recombination to yield potential disease loci. This approach has largely been applied to common, complex conditions for which many have hypothesized that a combination of common variants can influence genetic susceptibility to disease expression (Reich and Lander, 2001; Wang et al., 2005).

More recent studies, however, have uncovered a rare variant contribution to some apparently complex conditions (*i.e*. chronic kidney disease, scoliosis, arthrogryposis, developmental delay and intellectual disability), suggesting that a substantial proportion of seemingly common, complex conditions may in fact represent a combination of individually rare, Mendelian disease traits (Groopman et al., 2020; Karaca et al., 2015; Mitani et al., 2021; Pehlivan et al., 2019; Wu et al., 2015). These observations, and the elucidation of the *de novo* mutation contribution to rare disease across a range of phenotypes referred for study in diagnostic laboratories (Posey et al., 2019; Scott et al., 2021; Yang et al., 2013; Yang et al., 2014), lend support to the Clan Genomics hypothesis, which predicts that a disproportionate fraction of human disease is driven by new mutations that, by definition, are unique to a studied family or clan (Lupski, 2021; 2022; Lupski et al., 2011).

The role of new mutation in recessively inherited conditions has been less studied, although reports of novel variants contributing to recessive disease have been described in several population-specific cohorts (Alkuraya, 2010a; b; 2021). To comprehensively investigate the role of new mutation in recessive disease, we created a population-specific rare disease cohort and rare variant database against which to measure population-based frequencies in the context of population genetic substructure. The transmission of traits, genes and variant alleles from one generation to the next, may result in identity-by-descent (IBD) at a locus in a population characterized by consanguinity or founder effect due to a historical population bottleneck or geographic isolation. Experimentally, evidence for IBD in an individual genome is suggested by the presence of runs of homozygosity (ROH) not accompanied by copy-number variation; i.e. copy number neutral gene dosage at a locus. ROH regions in an individual's genome can be detected by genome-wide SNP arrays or can be calculated from unphased exome sequencing (ES) data that may reveal an absence of heterozygosity (AOH) for specific genomic intervals; such AOH variant information can be used as a surrogate measure of the fraction of the genome undergoing IBD and calculation of a coefficient of consanguinity in the family.

Genome-wide analysis of ROH genomic intervals in individuals from various populations can inform population-level differences (McQuillan et al., 2008) and may provide clues about the demographic and evolutionary history of a population, clan, or nuclear family (Lupski *et al.*, 2011; Nothnagel et al., 2010). For instance, when considering the number of genomic intervals and size (measured genetically in cM and physically in Mb) of ROH in an individual genome, a higher number of loci showing ROH

(‘distributed ROH’) suggests a population bottleneck (Auton et al., 2009; Browning and Browning, 2015; Ceballos et al., 2018), while longer ROH regions (‘contiguous ROH’) suggests a high rate of consanguinity (Li et al., 2006). On the other hand, fewer and shorter stretches of ROH regions may indicate shared ancestry over tens or hundreds of generations (Kirin et al., 2010).

Analysis of ROH regions in an individual genome can be used to prioritize potential pathogenic variations at a gene locus and may unveil possible genetic susceptibility underlying disease (Lohmueller et al., 2008; Tennessen et al., 2012; Torkamani et al., 2012). In addition, the inter-individual variation in ROH total length and number has also been shown to contribute to genetic architecture of complex traits and diseases (Clark et al., 2019; Joshi et al., 2015; Keller et al., 2012; Yengo et al., 2019). Therefore, analysis of ROH regions can be an adjuvant analytical tool to address the genetic architecture of disease. For instance, homozygosity mapping has been a central and robust genetic approach for the identification of biallelic variants causing autosomal recessive (AR) disease traits. For the identified “disease gene” the locus resides in ROH blocks shared among affected individuals (Broman and Weber, 1999; Houwen et al., 1994; Lander and Botstein, 1987; Morton, 1991; Seelow et al., 2009; Smith, 1953). This approach was successfully used to map disease genes in consanguineous families with heterogeneous neurological disorders (Alazami et al., 2015), multisystem disorders (Alazami et al., 2008; Alazami et al., 2009), and inborn errors of metabolism (Alkuraya, 2010a; b; 2021). Furthermore, analysis of rare homozygous deleterious variants in ROH regions can elucidate the genetic heterogeneity and molecular mechanisms underlying Mendelian traits due to either multi-locus variation or oligogenic/polygenic recessive effects

(Ceballos *et al.*, 2018; Kaiser et al., 2015; Karaca et al., 2018; Katsanis et al., 2001; Kirin *et al.*, 2010; McQuillan *et al.*, 2008; Mitani *et al.*, 2021; Pehlivan *et al.*, 2019; Posey et al., 2017); and even provide a molecular genetic explanation for trait penetrance and variability of expression of disease (Bejjani et al., 1998) and evidence for potential modifying gene loci (Bejjani et al., 2000; Gonzaga-Jauregui et al., 2015; Gonzaga-Jauregui et al., 2020)

Both the frequency and the degree of relatedness for consanguineous marriages within populations vary in different geographic regions and countries around the globe; the highest documented frequency is found in Pakistan, reported as 60-76% (Hashmi, 1997) of unions. Although consanguineous families facilitate genetic locus mapping and disease gene discovery, many populations with a relatively high coefficient of consanguinity, such as the Turkish (TK) population (Bittles, 2001; Bittles and Black, 2010), have not been deeply investigated with genomic studies, including a paucity of clinical genomics studies.

The population of Turkey presents peculiar features compared to other Middle East countries. Besides having a high reported rate of consanguinity, 20.1% (Tuncbilek and Koc, 1994), Turkey is also often described as a geographic and social ‘bridge’ between Asia and Europe, an important hub of both ancient and contemporary population migration. Previous studies of healthy unrelated individuals from the Greater Middle East have demonstrated that the TK peninsula population is the most admixed among the other populations within that region (Scott et al., 2016). Such populations are expected to be presented with a richer gene pool, containing more rare homozygous deleterious variants in comparison to isolated populations; whether isolated by geographic or social

‘population bottlenecks’ (Erzurumluoglu et al., 2016). Population structure is relevant to disease because of individual pathogenic alleles confined and enriched within specific populations; however, its impact on rare (MAF <= .05), ultra-rare (<= 0.0001) (Hansen et al., 2019), or even private variants, or combinations of alleles at a genetic locus, to disease traits remains under explored. Taken together, despite its unique characteristics, the TK peninsula population variome and substructure have not been reported - nor has the TK population been deeply investigated with genomic studies for their potential impact on the genomic architecture of disease traits.

Here, we tested the Clan Genomics hypothesis in a population with a high rate of recessive disease. To determine the influences of both admixture and consanguinity on population genetic variation, genome dynamics, and the genetic architecture of disease, we generated and analyzed a variome from exome sequencing (ES) of 1,416 TK individuals recruited from throughout the country of Turkey. This cohort includes 773 unrelated clinically affected individuals with a wide variety of suspected Mendelian disease traits and 643 of an unrelated set of their unaffected relatives. We further carried out systematic genomic and phenotypic analysis of this population that might reveal key features of the TK population variome and substructure that impact the genetic and genomic architecture of disease in this TK cohort.

Results

The fine-scale population substructure of the TK cohort

To study finer-scale population substructure of the TK individuals in comparison to the African, East Asian, European and South Asian population samples from the 1000 Genomes Project, we performed the uniform manifold approximation and projection

(UMAP) dimension reduction method. The first and second main UMAP components separated the samples from African, East Asian, European, South Asian and TK populations. These studies showed that the TK genomes were distinct from the African, East Asian, South Asian populations, but closely clustered with the variome of European samples and consist of two main subpopulations (cluster 1 (N=235) and cluster 2 (N=1,181) individuals, Figure 1A and B).

To evaluate the population substructure of the TK individuals, we ran the unsupervised ADMIXTURE algorithm by k=5 clusters to minimize cross validation error. The admixture analysis results revealed that compared to the first cluster (N=235), the second cluster (N=1,181) demonstrated a higher fraction of East Asian, European, South Asian (Wilcoxon test one-tailed P-values= $1.39e^{-}4$, $2.88e^{-47}$ and $2.36e^{-25}$) and a lower fraction of Middle Eastern (Wilcoxon test one-tailed P-values= $2.36e^{-25}$) ancestry, but do not significantly differ from each other in the African ancestry component (P-values = 0.172 Supplementary Figure 1).

Comparison of the TK cohort variome to control for variant database bias

We next questioned how the population substructure was represented in the TK variome by examination of the characteristics of the distinct 3,024,990 variants present in TK individuals. We found that 2.6% (N=79,628) and 17.4% of those variants (N=527,528) are uniquely present in the TK unaffected cluster 1 or 2 individuals, and 13% (N=394,010) and 16.3% of those variants (N=493,079) are uniquely present in the TK affected cluster 1 or 2 individuals, respectively (Figure 2A). We then surveyed all variants of the TK variome in control variant databases including the genome aggregation database (gnomAD, https://gnomad.broadinstitute.org) (Karczewski et al., 2020) and the Greater

Middle Eastern (GME) variome (Scott *et al.*, 2016). Regarding the variome in the TK unaffecteds, the overall comparison of all distinct SNVs found showed that 27% and 26% of the unique variants in cluster 1 (N=660,255 variants) and cluster 2 individuals (N=1,845,686 variants) were present in the gnomAD variome. Intriguingly, only 10% and 5%, of the cluster 1 and 2 variants in the TK unaffecteds were present in the GME variome, respectively, underscoring the necessity of population-matched control databases to accurately assess variant minor allele frequency (Figure 2B and C and Supplementary Figure 2A and B).

We also performed similar analyses for the variome of TK affecteds (N=773). These studies demonstrated that 24% and 26% of cluster 1 (N=1,174,977 variants) and cluster 2 (N= 1,914,090) variants, respectively, were represented in the gnomAD database. Of note, only either 7% or 5% of the cluster 1 and cluster 2 variants were represented in the GME variome (Figure 2D and E and Supplementary Figure 2C and D). Aggregate TK exome variant data from clusters 1 and 2 are publicly available for analysis through a TK variome database (https://turkishvariomedb.shinyapps.io/tvdb/).

Observation of higher estimated inbreeding coefficient values in the TK subjects

To obtain a more objective experimental measure of the consanguinity level, we estimated the inbreeding coefficient (F) values from ES data of the TK affecteds (N=773) and unaffecteds (N=643) in comparison to the African (N=661), East Asian (N=504), European (n=503) and South Asian (N=489) population samples from the 1000 Genomes Project. These analyses revealed that the estimated F values in the TK unaffecteds were significantly higher with mean values of 0.017 and 0.029 in cluster 1 and cluster 2 individuals, respectively as compared to African (0.004), East Asian (-0.001), European

(-0.0006) and South Asian (0.012) (Figure 3A). We further showed the estimated F values of TK affected cluster 1 and cluster 2 individuals (mean=0.055 vs. 0.052) were increased significantly compared to the TK unaffected cluster 1 and cluster 2 individuals, respectively (Wilcoxon test one-tailed P-values 2.3e-6 and 2.2e-16, Figure 3A and B). On the other hand, we did not observe any significant cluster-specific differences in the estimated F values of both TK affected (Wilcoxon test one-tailed P-value 0.34) and TK unaffected individuals (Wilcoxon test one-tailed P-value 0.11, Figure 3B). Therefore, we merged these two clusters for further analyses. Our analysis also showed that the measured genomic inbreeding coefficients - the fraction of the genome covered by ROHs > 1.5 Mb (FROH) - are 0.048 and 0.030 on average in the TK affecteds and unaffecteds, respectively and these are nearly 1-1 proportional to the average estimated F values of the TK affecteds [0.053] and unaffecteds [0.028]. These findings support the hypothesis that the excess of homozygosity in the TK genomes was mostly shaped by ROHs (Figure 3C).

Enrichment of long-sized ROH genomic regions in TK cohort individuals

We then hypothesized that higher F values measured in the TK cohort correlate with an increased length and number of long-sized ROH regions that arose on recently configured "young" haplotypes due to recent parental relatedness. To achieve this, we first identified ROH regions from ES data using an informatics tool, BafCalculator (https://github.com/BCM-Lupskilab/BafCalculator) (Karaca *et al.*, 2018) that calculates genomic intervals with absence of heterozygosity, AOH, from unphased ES data as a surrogate measure of ROH. To obtain copy-number neutral ROH regions from the calculated ROH intervals, we excluded a subset of the apparent homozygous regions

caused by common variant CNV deletions. Applying Gaussian-mixture modeling using the mclust R package, we next classified the genomic intervals for ROH regions detected through BafCalculator into three length classes: short-sized (0.210-0.671 Mb), medium-sized (0.671-2.64 Mb) and long-sized ROHs (>2.64 Mb). To show that those ROH regions in these 3 different and discrete categories are not overlapping and formed by different factors (e.g. recent inbreeding and local recombination rate), we first examined the distribution of those ROH regions of long-, medium- and short-sized and observed that they were located in different parts of the genome, i.e. map to different genetic locus intervals and those regions were distributed non-uniformly across the genome as clearly visualized in the circos plot (Supplementary Figure 3). The non-uniform distribution of ROHs may be formed across the genome due to several physical properties of the human genome: they may involve some genes that are targets of positive selection in a population (Pemberton et al., 2012) or include small structural variant (SV) inversions that suppress recombination (Curtis et al., 2008; Porubsky et al., 2022).

We also examined the effect of local recombination rate on the formation of those ROHs of 3 different and discrete ROH size classes. In alignment with the finding that ROHs of long-sized, medium-sized and short-sized ROHs distributed in different parts of the genome (Supplementary Figure 3), we found that long-sized ROHs are more likely to contain human genome recombination cold spot regions (Hussin et al., 2015) compared to the medium-sized (Wilcoxon test one-tailed P-value=1.54e-13) and short-sized ROHs (Wilcoxon test one-tailed P-value=2.08e-29). Overall, our computational analyses showed that we uncovered 3 different and discrete ROH size classes that are not overlapping with each other (distributed in different parts of the genome) and specific

and meaningful for the TK cohort. In addition, our data support the notion that 'genome geography of recombination rates' [i.e. positions of 'coldspots' versus 'hotspots' for recombination] may influence genetic architecture in specific populations.

To investigate the effect of inbreeding level on the genetic architecture of disease traits, and to uncover which genomic regions are more contributory to disease phenotypes in the TK population, we first compared the ROH length distribution between the TK affecteds and unaffecteds. As expected, the TK affecteds (with an average of estimated F values=0.053) are presented with a higher level of estimated F values compared to TK unaffecteds (with an average of estimated F values=0.028) given that consanguinity is well established to be a risk factor for rare disorders. This increase in the estimated F levels in TK affected vs. unaffecteds was found to be reflected in an increase in the long-sized ROH total size (median=111.71 Mb vs. 34.41 Mb, Wilcoxon test one-tailed P-value=2.09e-18) and number (median=13 vs. 6, Wilcoxon test one-tailed P-value=6.14e-16), but not medium-sized and short-sized ROHs (Figure 4A and Supplementary Figure 4). In parallel and in conjunction with these analyses, we then performed a correlation analysis to explore the hypothesis that higher estimated F values observed in the TK cohort manifested in an increased genome-wide burden of long-sized (>2.64 Mb) ROHs. Our analysis revealed that as the estimated inbreeding levels increase in the TK affecteds, the genome-wide burden of long-sized ROHs increase (ρ=0.83, Supplementary Figure 5A), but not the genome-wide burden of medium-sized ROHs (ρ=0.29, Supplementary Figure 5B) and short-sized ROH segments (ρ=-0.25, Supplementary Figure 5C). This analysis supports the notion that recent inbreeding is most likely to contribute to the formation of long-sized ROHs, but

not the other defined categories (i.e., medium and short). Taken together, both analyses showed that as the estimated inbreeding levels increase within the TK cohort (TK affecteds vs. TK unaffecteds and within the TK affecteds), the genome-wide burden of long-sized ROH regions also increase.

We next examined specifically the characteristics of other ROH size categories. The total length of short-sized ROH regions, which result from short homozygous blocks on ancient haplotypes showed a moderate negative correlation with the estimated F values (Supplementary Figure 5C). Concordant with the lower estimated F values in the TK unaffecteds, the short-sized ROH regions in the unaffecteds were greater in total size (median=31 vs. 28.62 Mb, Wilcoxon test one-tailed P-value=2.41e-7) and higher in number (median=126 vs. 122, Wilcoxon test one-tailed P-value=7.65e-8) than those of affecteds (Supplementary Figure 4B). In contrast, medium-sized ROH regions that mostly arise due to background relatedness (McQuillan *et al.*, 2008; Pemberton *et al.*, 2012) were present in a slightly higher number in the TK unaffecteds compared to affecteds (median=34 vs. 32, Wilcoxon test one-tailed P-value=0.04) but did not differ significantly in total length (median=39.11 vs. 39.77 Mb, Wilcoxon test one-tailed P-value=0.199) between the TK affecteds and unaffecteds (Supplementary Figure 4A).

Taken together, these ROH analyses support the notion that long-, medium-, and short-sized ROH regions result from individual or personal genome population history and dynamics such as consanguinity level, or background relatedness (McQuillan *et al.*, 2008; Pemberton *et al.*, 2012) in nuclear families and clans. Of note, the TK affecteds show a significantly increased overall burden of ROH segments per genome compared to unaffecteds stemming from an increased genome-wide burden of long-sized ROHs.

Enrichment of predicted deleterious variants in long-sized ROH regions

We next tested the hypothesis that long-sized ROH regions that arose due to recent parental relatedness, would be enriched for rare homozygous deleterious variants because insufficient generational time would not yet have allowed for selective elimination of such detrimental alleles from a population (Pemberton and Szpiech, 2018; Szpiech et al., 2019; Szpiech et al., 2013). To test this, we first identified rare homozygous deleterious variants (MAF $\leq$ 0.05) predicted to be potentially deleterious, by selecting variants above a CADD PHRED-scaled score of >=15 and by utilizing a prediction tool algorithm, NMDescPredictor, to predict potential LoF variants (Coban-Akdemir et al., 2018). To account for variable mutation rates across different samples and genomic regions, we computed a variant density metric by normalizing the count of rare homozygous deleterious variants to the count of rare homozygous synonymous variants. Since ROH regions are likely to enable deleterious variation to exist in a homozygous form, we then investigated the contribution of ROH regions to deleterious variant density in the TK cohort, by grouping rare homozygous deleterious variants into four groups based on their genomic location. That is, variants within ROH regions in three different size categories (long-, medium- and short-sized) or outside of an ROH block (non-ROH). As expected, in both the TK affecteds and unaffecteds, we observed an increased level of mutational burden existing in ROH regions that was most striking in long-sized ROH regions, which are more likely to be shaped by young haplotype blocks including deleterious variation. This was followed by medium-sized, short-sized

ROH and non-ROH regions (Figure 4B). On the other hand, we observed a significantly increased level of rare homozygous deleterious variant density in the TK affecteds compared to unaffecteds that was most strikingly outlined in long-sized (Wilcoxon test one-tailed P-value= 3.35e-11) and to a lesser extent in medium-sized ROHs (Wilcoxon test one-tailed P-value= 1.9e-9) and non-ROHs (Wilcoxon test one-tailed P-value= 4.36e-2, Figure 4B). On the other hand, short-sized ROHs do not seem to contribute to the overall rare homozygous deleterious variant density difference observed in ROH regions between the TK affecteds and unaffecteds (Wilcoxon test one-tailed P-value= 1.75e-1, Figure 4B).

We also tested the effect of local recombination rate on not only shaping the lengths of ROHs but also the accumulation of deleterious variation retrieving the annotations of CS and HS exonic regions of recombination from the previously published study (Hussin *et al.*, 2015). When we overlapped those regions with different ROH classes in each TK individual, we observed that the long-sized ROH regions are 5.76 times more likely to present with CS exonic regions compared to HS exonic regions of recombination. These numbers were 4.03, 3.56 and 1.89 for medium-sized, short-sized and non-ROH regions, respectively (Supplementary Figure 6). We also replicated the finding that CS exonic regions of recombination are more likely (1.24 times) to rare contain deleterious variation compared with HS exonic regions of recombination in a TK affected individual (Hussin *et al.*, 2015). Thus, recombination rate architecture of the human genome in the TK population may be one of the other potential explanations for the increased deleterious variant density in long-sized ROH regions in the TK affected individuals given that those regions contain a higher density

of CS exonic regions of recombination that more likely encompass rare and deleterious variation.

In summary, this analysis documented that long-sized ROHs were most enriched for rare homozygous deleterious variation compared to medium-sized, short-sized and non-ROHs irrespective of affection status in the TK cohort, indicating a contribution of recent parental relatedness to mutational burden in the TK population (Figure 4B). This further demonstrated that the overall burden of rare homozygous deleterious variation was significantly increased in TK affecteds compared to unaffecteds and most prominent in long-sized ROHs, conceptually reflecting copy number neutral structural variant haplotypes derived by new mutation and present with low rates of recombination in recent ancestors of the clan; e.g. analogous to SV haplotypes by *de novo Alu-Alu* mediated rearrangements (AAMR) generated as exonic deletion CNV alleles in the clan (Duan et al., 2021).

Phenotypic and population structure characterization of a mixed disease cohort

The TK subjects were recruited into the BHCMG because of suspected Mendelian disorders and presented with a wide variety of clinical phenotypes. To define the range and spectrum of clinical phenotypes, and the genetic traits observed in these individuals, we generated a phenotypic similarity score using the R package ontologySimilarity (James et al., 2016; Liu et al., 2019b; Posey *et al.*, 2017) and the Resnik approach to information content (Resnik, 1995) to evaluate semantic similarity in a taxonomy between each pair of individuals using the Human Phenotype Ontology (HPO) terms (Groza et al., 2015; Kohler et al., 2014) recorded in PhenoDB. We performed an unsupervised clustering of those subjects based on this phenotypic similarity score, revealing five major

‘disease phenotype groups’ in the TK affected individuals. Clusters 1, 3, and 4 consist mainly of individuals with diverse phenotypic features, which do not fit into a ‘singular general disease category or group’, i.e. higher order HPO term or generalizable disease state or clinical diagnosis. Clusters 2 and 4 are formed of individuals who could be grouped by defined clinical entities largely reflective of complex disease traits, including the hypergonadotropic hypogonadism (HH) cohort (Jolly et al., 2019) and the neurological disorders cohort (Karaca *et al.*, 2015), respectively (Figure 5A).

Genotype-phenotype analyses revealing ROH-associated genetic architecture of diseases

We then tested the extent to which mutational burden caused by rare homozygous deleterious variants in long-sized ROH regions explains clinical phenotypic features of the individuals in the TK cohort. To achieve this, we performed an unbiased genotype-phenotype correlation analysis based on the HPO terms (Herman et al., 2022; Zhang et al., 2022). In this analysis, we first linked the disease genes present with rare coding homozygous and deleterious variation in an individual genome to their related HPO terms for the trait, as defined in the OMIM (https://www.omim.org) clinical synopsis, according to HPO annotation resource databases. Then, for the clinical phenotypic features of each patient recorded in PhenoDB (Hamosh et al., 2013; Sobreira et al., 2015; Wohler E., 2021), we compared the associated HPO term sets to the merged HPO term sets for the disease genes defined for each ROH category, using a semantic similarity score metric that controls for the number of genes and ROH block size using a permutation approach (James et al., 2016; Liu et al., 2019b; Posey et al., 2017). These analyses showed that, in TK affected individuals, genes with rare homozygous

deleterious variants in long-sized ROH regions are most informative for clinical phenotypic features objectively assessed and compared, using the information submitted to and collated within PhenoDB (Hamosh et al., 2013; Sobreira et al., 2015; Wohler E., 2021) compared to medium-sized ROHs (P-value=1.7e-1), short-sized ROHs (P-value=1.2e-3) and non-ROHs (P-value=5e-2) (Figure 5B).

These analyses also revealed that the top-ranking genes with rare coding homozygous deleterious variant were located in the long-sized ROH regions in 152 patients (phenotypic similarity score >=1). Importantly, 75 out of those 152 patients were found to carry rare coding homozygous and deleterious variation located in >=2 OMIM disease genes that contribute significantly to the patients' phenotypes on the basis of phenotypic similarity score (score>=1). In line with these findings, we indicate a subset of the TK affecteds in the cohort present with neurodevelopmental disorders (NDD; N=234) that were analyzed by expert clinicians. In 176 of those 234 studied subjects (75.2%), a plausible and genetically parsimonious molecular etiology due to rare coding variation was identified. Importantly, out of those 176 subjects, 51 families (51/176 = 28.9%) were identified with multilocus pathogenic variation (MPV), mostly driven by ROHs (Mitani *et al.*, 2021). The retrospective analysis of those 176 subjects revealed that cases with diagnoses involving >=2 disease gene loci (N=51) were found to have significantly higher F values (Wilcoxon test one-tailed P-value= 9.35e-5, Figure 6A) and significantly increased total span of long-sized ROHs (Wilcoxon test one-tailed P-value=1.06e-4, Figure 6B) compared to cases with diagnoses involving one (1) disease gene locus. On the other hand, we found that there were no significant differences between these two groups of patients in terms of total span of medium-sized

ROHs (Wilcoxon test one-tailed P-value=0.223, Figure 6C). In summary, our results provide compelling evidence that an increased level of consanguinity observed in the TK affecteds compared to unaffecteds is correlated with a greater total span of long-sized ROH blocks and significantly increased level of rare homozygous deleterious variant density, thereby an elevated mutational burden that likely contributes to the disease trait(s) phenotype observed in the individuals studied.

In summary, our results provide evidence that an increased level of consanguinity observed in the TK affecteds compared to unaffecteds is correlated with a greater total span of long-sized ROH blocks and significantly increased level of rare homozygous deleterious variant density, thereby an elevated mutational burden that likely contributes to the disease trait phenotype observed in the individuals studied.

Discussion

Applications of ES and genome sequencing (GS) in research and the clinic, in order to unravel rare and pathogenic variation in the genome that contributes to biological perturbations from homeostasis underlying Mendelian disease traits, have enabled molecular diagnoses for hundreds of thousands of patients and also facilitated novel disease gene discovery (Bayram et al., 2016; Chong et al., 2015; de Ligt et al., 2012; Dharmadhikari et al., 2019; Eldomery et al., 2017; Karaca *et al.*, 2015; Lee et al., 2014; Liu *et al.*, 2019b; Lupski et al., 2010; Mitani *et al.*, 2021; Pehlivan *et al.*, 2019; Worthey et al., 2011; Yang *et al.*, 2013; Yang *et al.*, 2014), especially through the Centers for Mendelian Genomics program and other national and international organized efforts (Deciphering Developmental Disorders, 2015; Posey *et al.*, 2019; Sawyer et al., 2016). Comprehensive catalogues of common and rare human genetic variation stored in

population variant databases, such as ExAC (Lek et al., 2016), gnomAD (Karczewski *et al.*, 2020) (https://gnomad.broadinstitute.org), and ARIC (Coban-Akdemir *et al.*, 2018; Gambin et al., 2015), have proven to be powerful resources and interpretive tools to identify rare, ultra-rare, and pathogenic variation that influences gene action and expression of Mendelian disease traits. However, there remain many world populations for which genetic variation is underrepresented or entirely absent in such databases, including populations with more prevalent consanguinity and a considerable amount of admixture, such as the TK population (Tuncbilek and Koc, 1994).

Here, we characterized and examined the influences of both admixture and consanguinity on population genetic and genomic variation, substructure and genomic architecture of disease traits in a Turkish (TK) population cohort of 1,416 unrelated individuals. Characterization of this population by UMAP analysis demonstrated greatest similarity with the European population, with elucidation of two TK clusters (cluster 1, N=285; cluster 2, N=1,131) that demonstrated distinct patterns of admixture, underscoring the heterogeneity of this cohort (Figure 1C and Supplementary Figure 1). This heterogeneity was further revealed by an analysis of each cluster's variome (Figure 2A), which contained a substantial proportion (36.4%) of ultrarare variants (Hansen *et al.*, 2019) unique to each cluster, and not present in other population databases, highlighting the interpretive power of population-matched rare variant database to human disease research. Despite these differences in admixture and variomes between clusters, they shared similar estimated inbreeding levels, long-sized ROH burden and deleterious variant density (Figure 3B, Supplementary Figures 7 and 8). The underrepresentation of the TK variome variants in these control databases are expected

given the fact only 140 of 1,111 unrelated subjects were of TK ancestry in the GME variome (Scott *et al.*, 2016) and only 1,088 of 141,456 unrelated subjects were of Middle Eastern origin in the gnomAD database (Karczewski *et al.*, 2020).

Beyond the elucidation of the biological basis and molecular pathogenesis of disease, the mapping of a locus at which variation might contribute to disease analysis and characterization of molecular features in personal genomes can potentially provide some insights into the genetic architecture contributing to disease traits in a population and evolution of personal genomes. Using a TK population cohort, we show that investigation of the molecular features of ROH regions culled from personal unphased ES data through BafCalculator (https://github.com/BCM-Lupskilab/BafCalculator) (Karaca et al., 2018) and classified through Gaussian-mixture machine learning modeling into three length ROH classes specific to the TK population can provide insights into the haplotype derivation and genetic architecture of disease. Long-sized ROH (>2.64 Mb) regions that arose on recently configured haplotype blocks were greater in size (both total and median length) and number in the genomes of the TK affecteds compared to TK unaffecteds (median=111.71 Mb vs. 34.41 Mb, Wilcoxon test one-tailed P-value=2.09e-18 and median=13 vs. 6, Wilcoxon test one-tailed P-value=6.14e-16) without any significant cluster-specific differences (Figure 4A and Supplementary Figure 7). This finding is concordant with higher estimated F values (0.053 vs. 0.028, Wilcoxon test one-tailed P-value= $2.35e^{-18}$) and high level of consanguinity due to recent shared ancestors in the TK population (Scott et al., 2016). Characterization of ROH genomic intervals also revealed that long-sized ROH regions on newly derived haplotypes are particularly enriched with rare homozygous deleterious

variants specifically in the TK affecteds compared to TK unaffecteds (Wilcoxon test one-tailed P-value= 3.35e-11). Our analysis also uncovered that recombination rate architecture of the human genome in the TK population may also explain the increased deleterious variant density in long-sized ROH regions in the TK affected individuals given that those regions present with a higher density of CS exonic regions of recombination that more likely encompass rare and deleterious variation (Supplementary Figure 6). We also showed that as the estimated inbreeding levels increase in the TK affecteds, the rare homozygous deleterious variation density in long-sized ROHs also increase (ρ=0.4, Supplementary Figure 9). These findings support the notion that the inbreeding level alters the genetic architecture of disease traits in the TK population through an increase in the genome-wide burden of long-sized ROH along with an increase in their rare homozygous deleterious variation density (Figure 4A and B, and Supplementary Figure 9).

To test the contribution of those ROH-derived rare variant combinations to Mendelian phenotypes, we performed a large-scale analysis of genotype-phenotype correlations in the TK cohort from their clinical features captured as structured human phenotype ontology (HPO) terms (Groza *et al.*, 2015; Kohler *et al.*, 2014) (https://hpo.jax.org/app/download/annotation) recorded in PhenoDB (Wohler E., 2021) . A systematic, integrative quantitative analysis revealed that the combinatorial phenotypic effect of ultra-rare variants embedded within long-size ROH regions are most explanatory for the observed rare disease trait(s) in the TK cohort . Corroborating these data analyses findings, a retrospective analysis of previously published cases (N=176) (Bayram *et al.*, 2016; Karaca *et al.*, 2015; Mitani *et al.*, 2021; Pehlivan *et al.*, 2019) demonstrated that the

cases with multi-locus pathogenic variation (MPV; N=51) (diagnoses involving >=2 disease gene loci) are more likely to have an increased genome-wide burden of long-sized ROH regions (Wilcoxon test one-tailed P-value=1.06e-4, Figure 6B), corresponding to higher estimated F values (Wilcoxon test one-tailed P-value= 9.35e-5, Figure 6A) compared to cases with diagnoses involving 1 disease gene locus. That these variants were ultra-rare within the TK population itself suggests that they may represent new mutation events within individual families or the clan, the most basic unit of a population. Population substructure ultimately driving formation of these newly configured – and unique – disease haplotypes that can be rapidly brought to homozygosity through IBD: each shaped by recombination, characterized by new mutation, and even more rare than their constituent alleles (Narasimhan et al., 2017).

This phenomenon of new mutations as ultra-rare variants on a newly derived haplotype may provide important insights into the molecular etiology of disease traits, and further amplify several prior observations including: (1) the role of multilocus variation underlying some cases of apparent phenotypic expansion (Karaca *et al.*, 2018; Liu *et al.*, 2019b; Pehlivan *et al.*, 2019; Posey *et al.*, 2017); (2) homozygosity of ultra-rare pathogenic variation in *PRUNE* in sect-driven population isolates (Karaca *et al.*, 2015; Nistala et al., 2021; Zollo et al., 2017) in stark contrast with the contribution of rare (but not ultra-rare) *CLP1* founder alleles to microcephaly and neurodevelopmental disease (Karaca et al., 2014; Schaffer et al., 2014); (3) the seemingly now-common identification of genes for which biallelic variation can lead to disease traits previously categorized as strictly ‘dominant Mendelian loci’-traits (Mitani *et al.*, 2021; Monies et al., 2019; Rainger et al., 2014; Yuan et al., 2015), and (4) the emergence of a founder allele arisen by

identity-by-state (IBS) in Steel syndrome of the geographically isolated population of the Island of Puerto Rico versus clan genomics derived *COL27A1* pathogenic variation in the TK population (Gonzaga-Jauregui *et al.*, 2020).

Our findings also highlight the advantage of merging per-locus variation with genomics (inherited vs. *de novo* mutations) for gleaning insights into the genetic architecture contributing to disease in a population. Multiple genetic changes could be brought together per locus to generate unique haplotype blocks. This phenomenon could be exemplified by the observation of uniparental isodisomy (UPD) manifest by a long tract of homozygosity on the entirety of chromosome 7 explaining both the short stature phenotype in addition to the expected clinical features of cystic fibrosis (CF, OMIM #219700) in a child (Spence et al., 1988). Viewed from such a perspective, disease phenotypes resulting from UPD, and epigenetic/imprinting diseases may benefit from haplotype phased genomes and long read technologies that differentiate methylated W-C bases (Carvalho et al., 2019; Lupski et al., 2020). Another example of per-locus genetic studies is the modulation of disease risk through gene expression and dosage effects of regulatory common variant (expression quantitative trait loci, eQTLs) haplotype configurations of coding pathogenic variants and CNVs (Castel et al., 2018; Duan et al., 2022; Liu et al., 2019a; Ren et al., 2020; Wu *et al.*, 2015; Yang et al., 2019). The high mutation rate of recurrent genomic deletions (e.g., driven by a special type of mutational mechanism, nonallelic homologous recombination (NAHR)) may make these loci a significant contributor to AR disease trait loci in populations due to a compound heterozygous CNV + SNV allelic combination(Yuan, 2021).

This unique combination of rare variants located in ROH regions in each individual genome to generate disease haplotypes characteristic of their recent family lineage, pedigree, or clan may explain their clinical phenotypic features and thereby their pathogenicity, providing further support for the Clan Genomics hypothesis (Lupski, 2021; 2022; Lupski *et al.*, 2011) and potentially illuminating La Reunion paradox. This paradox was reported in previous studies that documented six different Limb-Girdle Muscular Dystrophy 2A (LGMD2A) gene mutations in a small genetic isolate from La Reunion Island, in which all affected individuals from La Reunion were hypothesized to share a common haplotype (Beckmann, 1996; Richard et al., 1995; Zlotogora et al., 1996); however, paradoxically, haplotype analysis demonstrated multiple haplotypes associating with disease (Allamand et al., 1995). This observation led to the generation of several alternative hypotheses, including a proposal by Zlotoroga et al (Zlotogora *et al.*, 1996) that multiple recent, independent occurrences of calpain mutations might explain this observation. Others in the field argued that this hypothesis would require both a high mutation rate, and a selective carrier advantage, for a population to rapidly gain and maintain multiple distinct variants within a locus (Beckmann, 1996). The 'paradox' has stood for decades in the literature without resolution.

In the present study, we provide compelling evidence to more systematically address the observed paradox: the rapid homozygosing of alleles through IBD in the setting of the most basic (family/Clan) unit of a population results in the expression of human disease due to private or ultra-rare variant (Hansen *et al.*, 2019) (rather than founder) alleles arising within a clan. The disease associated haplotypes escape Hardy-Weinberg equilibrium and its attendant principles, and thus forgoing the need for high

mutation rates or selective carrier advantage to maintain pathogenic alleles within the population.

To apply a 'merging' of genetics (per locus variation) and genomics (inherited 'variome' and *de novo* mutations) thinking in the clinic, our data emphasize identifying and systematically analyzing the ROH genomic intervals culled from the patient's personal unphased ES data using BafCalculator (https://github.com/BCM-Lupskilab/BafCalculator) (Karaca *et al.*, 2018). If the degree of parental relatedness as judged by the ROH size culled from unphased ES data suggests that the patient may come from a clan with a high estimated coefficient of consanguinity, rare homozygous variants mapping within the ROH regions and their combinatorial effect should be prioritized in molecular diagnoses (Karaca *et al.*, 2018; Liu *et al.*, 2019b; Pehlivan *et al.*, 2019; Posey *et al.*, 2017). Culling ROH regions from unphased clinical ES data using BafCalculator (https://github.com/ BCM-Lupskilab/BafCalculator) (Karaca *et al.*, 2018) may also enhance the discovery of pathogenic homozygous or hemizygous exonic CNV deletions arising on newly derived structural variant (SV) haplotypes in a clan homozygosed by IBD (Dharmadhikari *et al.*, 2019; Gambin et al., 2017; Karolak et al., 2019; Yuan et al., 2020).

In summary, we provide compelling evidence suggesting that ultra-rare (recently arisen) genomic variants in a clan evolve newly derived disease haplotypes that could potentially become homozygosed due to IBD in a given population. Our data demonstrate that such haplotypes, and the combinatorial effect of their embedded ultra-rare variants, are the most explanatory for the TK individuals' observed disease traits. Such haplotype

evolution, when placed in the population substructure context of IBD, results in homozygosity of disease haplotypes.

Acknowledgments

We thank all patients, their families, and their referring physicians who submitted samples for genomic studies. No additional compensation was offered for these studies. Funding: this work was supported in part by the US National Human Genome Research Institute (NHGRI)/National Heart Lung and Blood Institute (NHLBI) grant number UM1HG006542 to the Baylor Hopkins Center for Mendelian Genomics (BHCMG) (DV and JRL), the National Institute of Neurological Disorders and Stroke (NINDS) R35NS105078 (JRL), and the National Human Genome Research Institute U54-HG003273 (RAG). JEP was supported by NHGRI K08 HG008986.

Author Contributions

Z.C.A., X.S., F.C. D.P. and J.R.L. designed the study, analyzed the data, and drafted the manuscript. D.P., E.K., and Y.B. evaluated the clinical studies and the ascertainment and collection of samples from Turkey. A.H, V.R.S, R.A.L. and N.S. supervised the clinical data generation of PhenoDB entries of TK and non-TK subjects. J.R.L. and D.V. supervised the study. S.N.J., T.G., C.M.B.C., D.M.M., P.L, E.B., R.A.G., C.A.S., J.E.P. generated ES data and advised the sequencing and variant data analyses. All contributing co-authors have read, edited, and approved the final manuscript.

Declaration of Interests

J.R.L. has stock ownership in 23andMe, is a paid consultant for the Regeneron Genetics Center, and is a co-inventor on multiple United States and European patents related to molecular diagnostics for inherited neuropathies, eye diseases, genomic disorders, and

bacterial genomic fingerprinting. P.L. is an employee of Baylor College of Medicine and derives partial support through a professional services agreement with the Baylor Genetics (BG). The Department of Molecular and Human Genetics at Baylor College of Medicine derives revenue from molecular genetic and genomic testing (ES, GS, CMA, aCGH) offered at BG (http://www.bcm.edu/geneticlabs/). JRL serves on the SAB of BG. The other authors declare no competing financial interests.

References

Alazami, A.M., Al-Saif, A., Al-Semari, A., Bohlega, S., Zlitni, S., Alzahrani, F., Bavi, P., Kaya, N., Colak, D., Khalak, H., et al. (2008). Mutations in *C2orf37*, encoding a nucleolar protein, cause hypogonadism, alopecia, diabetes mellitus, mental retardation, and extrapyramidal syndrome. Am J Hum Genet *83*, 684–691. 10.1016/j.ajhg.2008.10.018.

Alazami, A.M., Patel, N., Shamseldin, H.E., Anazi, S., Al-Dosari, M.S., Alzahrani, F., Hijazi, H., Alshammari, M., Aldahmesh, M.A., Salih, M.A., et al. (2015). Accelerating novel candidate gene discovery in neurogenetic disorders via whole-exome sequencing of prescreened multiplex consanguineous families. Cell Rep *10*, 148–161. 10.1016/j.celrep.2014.12.015.

Alazami, A.M., Shaheen, R., Alzahrani, F., Snape, K., Saggar, A., Brinkmann, B., Bavi, P., Al-Gazali, L.I., and Alkuraya, F.S. (2009). *FREM1* mutations cause bifid nose, renal agenesis, and anorectal malformations syndrome. Am J Hum Genet *85*, 414–418. 10.1016/j.ajhg.2009.08.010.

Alkuraya, F.S. (2010a). Autozygome decoded. Genet Med *12*, 765–771. 10.1097/GIM.0b013e3181fbfcc4.

Alkuraya, F.S. (2010b). Homozygosity mapping: one more tool in the clinical geneticists toolbox. Genet Med *12*, 236–239. 10.1097/GIM.0b013e3181ceb95d.

Alkuraya, F.S. (2021). How the human genome transformed study of rare diseases. Nature *590*, 218–219. 10.1038/d41586-021-00294-7.

Allamand, V., Broux, O., Richard, I., Fougerousse, F., Chiannilkulchai, N., Bourg, N., Brenguier, L., Devaud, C., Pasturaud, P., Pereira de Souza, A., and et al. (1995). Preferential localization of the limb-girdle muscular dystrophy type 2A gene in the proximal part of a 1-cM 15q15.1-q15.3 interval. Am J Hum Genet *56*, 1417–1430.

Auton, A., Bryc, K., Boyko, A.R., Lohmueller, K.E., Novembre, J., Reynolds, A., Indap, A., Wright, M.H., Degenhardt, J.D., Gutenkunst, R.N., et al. (2009). Global distribution of genomic diversity underscores rich complex history of continental human populations. Genome Res *19*, 795–803. 10.1101/gr.088898.108.

Bainbridge, M.N., Wiszniewski, W., Murdock, D.R., Friedman, J., Gonzaga-Jauregui, C., Newsham, I., Reid, J.G., Fink, J.K., Morgan, M.B., Gingras, M.C., et al. (2011). Whole-genome sequencing for optimized patient management. Sci Transl Med *3*, 87re83. 10.1126/scitranslmed.3002243.

Bayram, Y., Karaca, E., Coban Akdemir, Z., Yilmaz, E.O., Tayfun, G.A., Aydin, H., Torun, D., Bozdogan, S.T., Gezdirici, A., Isikay, S., et al. (2016). Molecular etiology of

arthrogryposis in multiple families of mostly Turkish origin. J Clin Invest *126*, 762–778. 10.1172/JCI84457.

Beckmann, J.S. (1996). The Reunion paradox and the digenic model. Am J Hum Genet *59*, 1400–1402.

Bejjani, B.A., Lewis, R.A., Tomey, K.F., Anderson, K.L., Dueker, D.K., Jabak, M., Astle, W.F., Otterud, B., Leppert, M., and Lupski, J.R. (1998). Mutations in *CYP1B1*, the gene for cytochrome P4501B1, are the predominant cause of primary congenital glaucoma in Saudi Arabia. Am J Hum Genet *62*, 325–333. 10.1086/301725.

Bejjani, B.A., Stockton, D.W., Lewis, R.A., Tomey, K.F., Dueker, D.K., Jabak, M., Astle, W.F., and Lupski, J.R. (2000). Multiple *CYP1B1* mutations and incomplete penetrance in an inbred population segregating primary congenital glaucoma suggest frequent de novo events and a dominant modifier locus. Hum Mol Genet *9*, 367–374. 10.1093/hmg/9.3.367.

Bittles, A. (2001). Consanguinity and its relevance to clinical genetics. Clin Genet *60*, 89–98.

Bittles, A.H., and Black, M.L. (2010). Evolution in health and medicine Sackler colloquium: Consanguinity, human evolution, and complex diseases. Proc Natl Acad Sci U S A *107 Suppl 1*, 1779–1786. 10.1073/pnas.0906079106.

Broman, K.W., and Weber, J.L. (1999). Long homozygous chromosomal segments in reference families from the centre dEtude du polymorphisme humain. Am J Hum Genet *65*, 1493–1500. 10.1086/302661.

Browning, S.R., and Browning, B.L. (2015). Accurate Non-parametric Estimation of Recent Effective Population Size from Segments of Identity by Descent. Am J Hum Genet *97*, 404–418. 10.1016/j.ajhg.2015.07.012.

Carvalho, C.M.B., Coban-Akdemir, Z., Hijazi, H., Yuan, B., Pendleton, M., Harrington, E., Beaulaurier, J., Juul, S., Turner, D.J., Kanchi, R.S., et al. (2019). Interchromosomal template-switching as a novel molecular mechanism for imprinting perturbations associated with Temple syndrome. Genome Med *11*, 25. 10.1186/s13073-019-0633-y.

Castel, S.E., Cervera, A., Mohammadi, P., Aguet, F., Reverter, F., Wolman, A., Guigo, R., Iossifov, I., Vasileva, A., and Lappalainen, T. (2018). Modified penetrance of coding variants by cis-regulatory variation contributes to disease risk. Nat Genet *50*, 1327–1334. 10.1038/s41588-018-0192-y.

Ceballos, F.C., Joshi, P.K., Clark, D.W., Ramsay, M., and Wilson, J.F. (2018). Runs of homozygosity: windows into population history and trait architecture. Nat Rev Genet *19*, 220–234. 10.1038/nrg.2017.109.

Challis, D., Yu, J., Evani, U.S., Jackson, A.R., Paithankar, S., Coarfa, C., Milosavljevic, A., Gibbs, R.A., and Yu, F. (2012). An integrative variant analysis suite for whole exome next-generation sequencing data. BMC Bioinformatics *13*, 8. 10.1186/1471-2105-13-8.

Chong, J.X., Buckingham, K.J., Jhangiani, S.N., Boehm, C., Sobreira, N., Smith, J.D., Harrell, T.M., McMillin, M.J., Wiszniewski, W., Gambin, T., et al. (2015). The Genetic Basis of Mendelian Phenotypes: Discoveries, Challenges, and Opportunities. Am J Hum Genet *97*, 199-215. 10.1016/j.ajhg.2015.06.009.

Clark, D.W., Okada, Y., Moore, K.H.S., Mason, D., Pirastu, N., Gandin, I., Mattsson, H., Barnes, C.L.K., Lin, K., Zhao, J.H., et al. (2019). Associations of autozygosity with a broad range of human phenotypes. Nat Commun *10*, 4957. 10.1038/s41467-019-12283-6.

Coban-Akdemir, Z., White, J.J., Song, X., Jhangiani, S.N., Fatih, J.M., Gambin, T., Bayram, Y., Chinn, I.K., Karaca, E., Punetha, J., et al. (2018). Identifying Genes Whose Mutant Transcripts Cause Dominant Disease Traits by Potential Gain-of-Function Alleles. Am J Hum Genet *103*, 171-187. 10.1016/j.ajhg.2018.06.009.

Curtis, D., Vine, A.E., and Knight, J. (2008). Study of regions of extended homozygosity provides a powerful method to explore haplotype structure of human populations. Ann Hum Genet *72*, 261-278. 10.1111/j.1469-1809.2007.00411.x.

de Ligt, J., Willemsen, M.H., van Bon, B.W., Kleefstra, T., Yntema, H.G., Kroes, T., Vulto-van Silfhout, A.T., Koolen, D.A., de Vries, P., Gilissen, C., et al. (2012). Diagnostic exome sequencing in persons with severe intellectual disability. N Engl J Med *367*, 1921-1929. 10.1056/NEJMoa1206524.

Deciphering Developmental Disorders, S. (2015). Large-scale discovery of novel genetic causes of developmental disorders. Nature *519*, 223-228. 10.1038/nature14135.

Dharmadhikari, A.V., Ghosh, R., Yuan, B., Liu, P., Dai, H., Al Masri, S., Scull, J., Posey, J.E., Jiang, A.H., He, W., et al. (2019). Copy number variant and runs of homozygosity detection by microarrays enabled more precise molecular diagnoses in 11,020 clinical exome cases. Genome Med *11*, 30. 10.1186/s13073-019-0639-5.

Duan, R., Hijazi, H., Bayram, Y., Karaca, E., Bertola, D.R., Isikay, S., Gulec, E.Y., Eker, H.K., Sahin, Y., Ocak, Z., et al. (2022). Developmental genomics of congenital limb malformations: further evidence for gene dosage effects *Human Genetics and Genomics Advances. In press.*

Duan, R., Saadi, N.W., Grochowski, C.M., Bhadila, G., Faridoun, A., Mitani, T., Du, H., Fatih, J.M., Jhangiani, S.N., Akdemir, Z.C., et al. (2021). A novel homozygous *SLC13A5* whole-gene deletion generated by Alu/Alu-mediated rearrangement in an Iraqi family with epileptic encephalopathy. Am J Med Genet A *185*, 1972-1980. 10.1002/ajmg.a.62192.

Eldomery, M.K., Coban-Akdemir, Z., Harel, T., Rosenfeld, J.A., Gambin, T., Stray-Pedersen, A., Kury, S., Mercier, S., Lessel, D., Denecke, J., et al. (2017). Lessons learned from additional research analyses of unsolved clinical exome cases. Genome Med *9*, 26. 10.1186/s13073-017-0412-6.

Erzurumluoglu, A.M., Shihab, H.A., Rodriguez, S., Gaunt, T.R., and Day, I.N. (2016). Importance of Genetic Studies in Consanguineous Populations for the Characterization of Novel Human Gene Functions. Ann Hum Genet *80*, 187-196. 10.1111/ahg.12150.

Farek, J., Hughes, D., Mansfield, A., Krasheninina, O., Nasser, W., Sedlazeck, F.J., Khan, Z., Venner, E., Metcalf, G., Boerwinkle, E., et al. (2018). xAtlas: Scalable small variant calling across heterogeneous next-generation sequencing experiments. BioRxiv.

Fromer, M., and Purcell, S.M. (2014). Using XHMM Software to Detect Copy Number Variation in Whole-Exome Sequencing Data. Curr Protoc Hum Genet *81*, 7 23 21-21. 10.1002/0471142905.hg0723s81.

Gambin, T., Akdemir, Z.C., Yuan, B., Gu, S., Chiang, T., Carvalho, C.M.B., Shaw, C., Jhangiani, S., Boone, P.M., Eldomery, M.K., et al. (2017). Homozygous and hemizygous CNV detection from exome sequencing data in a Mendelian disease cohort. Nucleic Acids Res *45*, 1633-1648. 10.1093/nar/gkw1237.

Gambin, T., Jhangiani, S.N., Below, J.E., Campbell, I.M., Wiszniewski, W., Muzny, D.M., Staples, J., Morrison, A.C., Bainbridge, M.N., Penney, S., et al. (2015). Secondary findings and carrier test frequencies in a large multiethnic sample. Genome Med *7*, 54. 10.1186/s13073-015-0171-1.

Gonzaga-Jauregui, C., Harel, T., Gambin, T., Kousi, M., Griffin, L.B., Francescatto, L., Ozes, B., Karaca, E., Jhangiani, S.N., Bainbridge, M.N., et al. (2015). Exome Sequence Analysis Suggests that Genetic Burden Contributes to Phenotypic Variability and Complex Neuropathy. Cell Rep *12*, 1169-1183. 10.1016/j.celrep.2015.07.023.

Gonzaga-Jauregui, C., Yesil, G., Nistala, H., Gezdirici, A., Bayram, Y., Nannuru, K.C., Pehlivan, D., Yuan, B., Jimenez, J., Sahin, Y., et al. (2020). Functional biology of the Steel syndrome founder allele and evidence for clan genomics derivation of *COL27A1* pathogenic alleles worldwide. Eur J Hum Genet *28*, 1243-1264. 10.1038/s41431-020-0632-x.

Groopman, E.E., Povysil, G., Goldstein, D.B., and Gharavi, A.G. (2020). Rare genetic causes of complex kidney and urological diseases. Nat Rev Nephrol *16*, 641-656. 10.1038/s41581-020-0325-2.

Groza, T., Kohler, S., Moldenhauer, D., Vasilevsky, N., Baynam, G., Zemojtel, T., Schriml, L.M., Kibbe, W.A., Schofield, P.N., Beck, T., et al. (2015). The Human Phenotype Ontology: Semantic Unification of Common and Rare Disease. Am J Hum Genet *97*, 111-124. 10.1016/j.ajhg.2015.05.020.

Hamosh, A., Sobreira, N., Hoover-Fong, J., Sutton, V.R., Boehm, C., Schiettecatte, F., and Valle, D. (2013). PhenoDB: a new web-based tool for the collection, storage, and analysis of phenotypic features. Hum Mutat *34*, 566-571. 10.1002/humu.22283.

Hansen, A.W., Murugan, M., Li, H., Khayat, M.M., Wang, L., Rosenfeld, J., Andrews, B.K., Jhangiani, S.N., Coban Akdemir, Z.H., Sedlazeck, F.J., et al. (2019). A Genocentric Approach to Discovery of Mendelian Disorders. Am J Hum Genet *105*, 974-986. 10.1016/j.ajhg.2019.09.027.

Hashmi, M.A. (1997). Frequency of consanguinity and its effect on congenital malformation--a hospital based study. J Pak Med Assoc *47*, 75-78.

Herman, I., Jolly, A., Du, H., Dawood, M., Abdel-Salam, G.M.H., Marafi, D., Mitani, T., Calame, D.G., Coban-Akdemir, Z., Fatih, J.M., et al. (2022). Quantitative dissection of multilocus pathogenic variation in an Egyptian infant with severe neurodevelopmental disorder resulting from multiple molecular diagnoses. Am J Med Genet A *188*, 735-750. 10.1002/ajmg.a.62565.

Houwen, R.H., Baharloo, S., Blankenship, K., Raeymaekers, P., Juyn, J., Sandkuijl, L.A., and Freimer, N.B. (1994). Genome screening by searching for shared segments: mapping a gene for benign recurrent intrahepatic cholestasis. Nat Genet *8*, 380-386. 10.1038/ng1294-380.

Huber, W., Carey, V.J., Gentleman, R., Anders, S., Carlson, M., Carvalho, B.S., Bravo, H.C., Davis, S., Gatto, L., Girke, T., et al. (2015). Orchestrating high-throughput genomic analysis with Bioconductor. Nat Methods *12*, 115-121. 10.1038/nmeth.3252.

Hussin, J.G., Hodgkinson, A., Idaghdour, Y., Grenier, J.C., Goulet, J.P., Gbeha, E., Hip-Ki, E., and Awadalla, P. (2015). Recombination affects accumulation of damaging and disease-associated mutations in human populations. Nat Genet *47*, 400-404. 10.1038/ng.3216.

James, R.A., Campbell, I.M., Chen, E.S., Boone, P.M., Rao, M.A., Bainbridge, M.N., Lupski, J.R., Yang, Y., Eng, C.M., Posey, J.E., and Shaw, C.A. (2016). A visual and curatorial approach to clinical variant prioritization and disease gene discovery in genome-wide diagnostics. Genome Med *8*, 13. 10.1186/s13073-016-0261-8.

Jolly, A., Bayram, Y., Turan, S., Aycan, Z., Tos, T., Abali, Z.Y., Hacihamdioglu, B., Coban Akdemir, Z.H., Hijazi, H., Bas, S., et al. (2019). Exome Sequencing of a Primary Ovarian Insufficiency Cohort Reveals Common Molecular Etiologies for a Spectrum of Disease. J Clin Endocrinol Metab *104*, 3049-3067. 10.1210/jc.2019-00248.

Joshi, P.K., Esko, T., Mattsson, H., Eklund, N., Gandin, I., Nutile, T., Jackson, A.U., Schurmann, C., Smith, A.V., Zhang, W., et al. (2015). Directional dominance on stature and cognition in diverse human populations. Nature *523*, 459-462. 10.1038/nature14618.

Kaiser, V. B., Svinti, V., Prendergast, J. G., Chau, Y. Y., Campbell, A., Patarcic, I., Barroso, I., Joshi, P. K., Hastie, N. D., Miljkovic, A., et al. (2015). Homozygous loss–of–function variants in European cosmopolitan and isolate populations. Hum Mol Genet *24*, 5464–5474. 10.1093/hmg/ddv272.

Karaca, E., Harel, T., Pehlivan, D., Jhangiani, S. N., Gambin, T., Coban Akdemir, Z., Gonzaga–Jauregui, C., Erdin, S., Bayram, Y., Campbell, I. M., et al. (2015). Genes that Affect Brain Structure and Function Identified by Rare Variant Analyses of Mendelian Neurologic Disease. Neuron *88*, 499–513. 10.1016/j.neuron.2015.09.048.

Karaca, E., Posey, J. E., Coban Akdemir, Z., Pehlivan, D., Harel, T., Jhangiani, S. N., Bayram, Y., Song, X., Bahrambeigi, V., Yuregir, O. O., et al. (2018). Phenotypic expansion illuminates multilocus pathogenic variation. Genet Med *20*, 1528–1537. 10.1038/gim.2018.33.

Karaca, E., Weitzer, S., Pehlivan, D., Shiraishi, H., Gogakos, T., Hanada, T., Jhangiani, S. N., Wiszniewski, W., Withers, M., Campbell, I. M., et al. (2014). Human *CLP1* mutations alter tRNA biogenesis, affecting both peripheral and central nervous system function. Cell *157*, 636–650. 10.1016/j.cell.2014.02.058.

Karczewski, K. J., Francioli, L. C., Tiao, G., Cummings, B. B., Alfoldi, J., Wang, Q., Collins, R. L., Laricchia, K. M., Ganna, A., Birnbaum, D. P., et al. (2020). The mutational constraint spectrum quantified from variation in 141,456 humans. Nature *581*, 434–443. 10.1038/s41586–020–2308–7.

Karolak, J. A., Vincent, M., Deutsch, G., Gambin, T., Cogne, B., Pichon, O., Vetrini, F., Mefford, H. C., Dines, J. N., Golden–Grant, K., et al. (2019). Complex Compound Inheritance of Lethal Lung Developmental Disorders Due to Disruption of the TBX–FGF Pathway. Am J Hum Genet *104*, 213–228. 10.1016/j.ajhg.2018.12.010.

Katsanis, N., Ansley, S. J., Badano, J. L., Eichers, E. R., Lewis, R. A., Hoskins, B. E., Scambler, P. J., Davidson, W. S., Beales, P. L., and Lupski, J. R. (2001). Triallelic inheritance in Bardet–Biedl syndrome, a Mendelian recessive disorder. Science *293*, 2256–2259. 10.1126/science.1063525.

Keller, M. C., Simonson, M. A., Ripke, S., Neale, B. M., Gejman, P. V., Howrigan, D. P., Lee, S. H., Lencz, T., Levinson, D. F., Sullivan, P. F., and Schizophrenia Psychiatric Genome–Wide Association Study, C. (2012). Runs of homozygosity implicate autozygosity as a schizophrenia risk factor. PLoS Genet *8*, e1002656. 10.1371/journal.pgen.1002656.

Kirin, M., McQuillan, R., Franklin, C. S., Campbell, H., McKeigue, P. M., and Wilson, J. F. (2010). Genomic runs of homozygosity record population history and consanguinity. PLoS One *5*, e13996. 10.1371/journal.pone.0013996.

Kohler, S., Doelken, S.C., Mungall, C.J., Bauer, S., Firth, H.V., Bailleul–Forestier, I., Black, G.C., Brown, D.L., Brudno, M., Campbell, J., et al. (2014). The Human Phenotype Ontology project: linking molecular biology and disease through phenotype data. Nucleic Acids Res *42*, D966–974. 10.1093/nar/gkt1026.

Lander, E.S., and Botstein, D. (1987). Homozygosity mapping: a way to map human recessive traits with the DNA of inbred children. Science *236*, 1567–1570.

Lee, H., Deignan, J.L., Dorrani, N., Strom, S.P., Kantarci, S., Quintero–Rivera, F., Das, K., Toy, T., Harry, B., Yourshaw, M., et al. (2014). Clinical exome sequencing for genetic identification of rare Mendelian disorders. JAMA *312*, 1880–1887. 10.1001/jama.2014.14604.

Lek, M., Karczewski, K.J., Minikel, E.V., Samocha, K.E., Banks, E., Fennell, T., ODonnell–Luria, A.H., Ware, J.S., Hill, A.J., Cummings, B.B., et al. (2016). Analysis of protein–coding genetic variation in 60,706 humans. Nature *536*, 285–291. 10.1038/nature19057.

Li, L.H., Ho, S.F., Chen, C.H., Wei, C.Y., Wong, W.C., Li, L.Y., Hung, S.I., Chung, W.H., Pan, W.H., Lee, M.T., et al. (2006). Long contiguous stretches of homozygosity in the human genome. Hum Mutat *27*, 1115–1121. 10.1002/humu.20399.

Liu, J., Wu, N., Deciphering Disorders Involving, S., study, C.O., Yang, N., Takeda, K., Chen, W., Li, W., Du, R., Liu, S., et al. (2019a). *TBX6*–associated congenital scoliosis (TACS) as a clinically distinguishable subtype of congenital scoliosis: further evidence supporting the compound inheritance and *TBX6* gene dosage model. Genet Med *21*, 1548–1558. 10.1038/s41436–018–0377–x.

Liu, P., Meng, L., Normand, E.A., Xia, F., Song, X., Ghazi, A., Rosenfeld, J., Magoulas, P.L., Braxton, A., Ward, P., et al. (2019b). Reanalysis of Clinical Exome Sequencing Data. N Engl J Med *380*, 2478–2480. 10.1056/NEJMc1812033.

Lohmueller, K.E., Indap, A.R., Schmidt, S., Boyko, A.R., Hernandez, R.D., Hubisz, M.J., Sninsky, J.J., White, T.J., Sunyaev, S.R., Nielsen, R., et al. (2008). Proportionally more deleterious genetic variation in European than in African populations. Nature *451*, 994–997. 10.1038/nature06611.

Lupski, J.R. (2021). Clan genomics: From OMIM phenotypic traits to genes and biology. Am J Med Genet A *185*, 3294–3313. 10.1002/ajmg.a.62434.

Lupski, J.R. (2022). Biology in balance: human diploid genome integrity, gene dosage, and genomic medicine. Trends Genet *38*, 554–571. 10.1016/j.tig.2022.03.001.

Lupski, J.R., Belmont, J.W., Boerwinkle, E., and Gibbs, R.A. (2011). Clan genomics and the complex architecture of human disease. Cell *147*, 32–43. 10.1016/j.cell.2011.09.008.

Lupski, J.R., Liu, P., Stankiewicz, P., Carvalho, C.M.B., and Posey, J.E. (2020). Clinical genomics and contextualizing genome variation in the diagnostic laboratory. Expert Rev Mol Diagn *20*, 995–1002. 10.1080/14737159.2020.1826312.

Lupski, J.R., Reid, J.G., Gonzaga–Jauregui, C., Rio Deiros, D., Chen, D.C., Nazareth, L., Bainbridge, M., Dinh, H., Jing, C., Wheeler, D.A., et al. (2010). Whole–genome sequencing in a patient with Charcot–Marie–Tooth neuropathy. N Engl J Med *362*, 1181–1191. 10.1056/NEJMoa0908094.

McQuillan, R., Leutenegger, A.L., Abdel–Rahman, R., Franklin, C.S., Pericic, M., Barac–Lauc, L., Smolej–Narancic, N., Janicijevic, B., Polasek, O., Tenesa, A., et al. (2008). Runs of homozygosity in European populations. Am J Hum Genet *83*, 359–372. 10.1016/j.ajhg.2008.08.007.

Mitani, T., Isikay, S., Gezdirici, A., Gulec, E.Y., Punetha, J., Fatih, J.M., Herman, I., Akay, G., Du, H., Calame, D.G., et al. (2021). High prevalence of multilocus pathogenic variation in neurodevelopmental disorders in the Turkish population. Am J Hum Genet *108*, 1981–2005. 10.1016/j.ajhg.2021.08.009.

Monies, D., Abouelhoda, M., Assoum, M., Moghrabi, N., Rafiullah, R., Almontashiri, N., Alowain, M., Alzaidan, H., Alsayed, M., Subhani, S., et al. (2019). Lessons Learned from Large–Scale, First–Tier Clinical Exome Sequencing in a Highly Consanguineous Population. Am J Hum Genet *104*, 1182–1201. 10.1016/j.ajhg.2019.04.011.

Morton, N.E. (1991). Genetic epidemiology of hearing impairment. Ann N Y Acad Sci *630*, 16–31.

Narasimhan, V.M., Rahbari, R., Scally, A., Wuster, A., Mason, D., Xue, Y., Wright, J., Trembath, R.C., Maher, E.R., van Heel, D.A., et al. (2017). Estimating the human mutation rate from autozygous segments reveals population differences in human mutational processes. Nat Commun *8*, 303. 10.1038/s41467–017–00323–y.

Nistala, H., Dronzek, J., Gonzaga–Jauregui, C., Chim, S.M., Rajamani, S., Nuwayhid, S., Delgado, D., Burke, E., Karaca, E., Franklin, M.C., et al. (2021). NMIHBA results from hypomorphic *PRUNE1* variants that lack short–chain exopolyphosphatase activity. Hum Mol Genet *29*, 3516–3531. 10.1093/hmg/ddaa237.

Nothnagel, M., Lu, T.T., Kayser, M., and Krawczak, M. (2010). Genomic and geographic distribution of SNP–defined runs of homozygosity in Europeans. Hum Mol Genet *19*, 2927–2935. 10.1093/hmg/ddq198.

Olshen, A.B., Venkatraman, E.S., Lucito, R., and Wigler, M. (2004). Circular binary segmentation for the analysis of array–based DNA copy number data. Biostatistics *5*, 557–572. 10.1093/biostatistics/kxh008.

Pehlivan, D., Bayram, Y., Gunes, N., Coban Akdemir, Z., Shukla, A., Bierhals, T., Tabakci, B., Sahin, Y., Gezdirici, A., Fatih, J.M., et al. (2019). The Genomics of Arthrogryposis, a Complex Trait: Candidate Genes and Further Evidence for Oligogenic Inheritance. Am J Hum Genet *105*, 132–150. 10.1016/j.ajhg.2019.05.015.

Pemberton, T.J., Absher, D., Feldman, M.W., Myers, R.M., Rosenberg, N.A., and Li, J.Z. (2012). Genomic patterns of homozygosity in worldwide human populations. Am J Hum Genet *91*, 275–292. 10.1016/j.ajhg.2012.06.014.

Pemberton, T.J., and Szpiech, Z.A. (2018). Relationship between Deleterious Variation, Genomic Autozygosity, and Disease Risk: Insights from The 1000 Genomes Project. Am J Hum Genet *102*, 658–675. 10.1016/j.ajhg.2018.02.013.

Porubsky, D., Hops, W., Ashraf, H., Hsieh, P., Rodriguez–Martin, B., Yilmaz, F., Ebler, J., Hallast, P., Maria Maggiolini, F.A., Harvey, W.T., et al. (2022). Recurrent inversion polymorphisms in humans associate with genetic instability and genomic disorders. Cell *185*, 1986–2005 e1926. 10.1016/j.cell.2022.04.017.

Posey, J.E., Harel, T., Liu, P., Rosenfeld, J.A., James, R.A., Coban Akdemir, Z.H., Walkiewicz, M., Bi, W., Xiao, R., Ding, Y., et al. (2017). Resolution of Disease Phenotypes Resulting from Multilocus Genomic Variation. N Engl J Med *376*, 21–31. 10.1056/NEJMoa1516767.

Posey, J.E., ODonnell–Luria, A.H., Chong, J.X., Harel, T., Jhangiani, S.N., Coban Akdemir, Z.H., Buyske, S., Pehlivan, D., Carvalho, C.M.B., Baxter, S., et al. (2019). Insights into genetics, human biology and disease gleaned from family based genomic studies. Genet Med *21*, 798–812. 10.1038/s41436–018–0408–7.

Quinlan, A.R. (2014). BEDTools: The Swiss–Army Tool for Genome Feature Analysis. Curr Protoc Bioinformatics *47*, 11 12 11–34. 10.1002/0471250953.bi1112s47.

Rainger, J., Pehlivan, D., Johansson, S., Bengani, H., Sanchez–Pulido, L., Williamson, K.A., Ture, M., Barker, H., Rosendahl, K., Spranger, J., et al. (2014). Monoallelic and biallelic mutations in *MAB21L2* cause a spectrum of major eye malformations. Am J Hum Genet *94*, 915–923. 10.1016/j.ajhg.2014.05.005.

Reich, D.E., and Lander, E.S. (2001). On the allelic spectrum of human disease. Trends Genet *17*, 502–510. 10.1016/s0168–9525(01)02410–6.

Reid, J.G., Carroll, A., Veeraraghavan, N., Dahdouli, M., Sundquist, A., English, A., Bainbridge, M., White, S., Salerno, W., Buhay, C., et al. (2014). Launching genomics into the cloud: deployment of Mercury, a next generation sequence analysis pipeline. BMC Bioinformatics *15*, 30. 10.1186/1471–2105–15–30.

Ren, X., Yang, N., Wu, N., Xu, X., Chen, W., Zhang, L., Li, Y., Du, R.Q., Dong, S., Zhao, S., et al. (2020). Increased *TBX6* gene dosages induce congenital cervical vertebral

malformations in humans and mice. J Med Genet *57*, 371–379. 10.1136/jmedgenet-2019-106333.

Resnik, P. (1995). Using information content to evaluate semantic similarity in a taxonomy. In: Proceedings of the 14th International Joint Conference on Artificial Intelligence, 448–453.

Richard, I., Broux, O., Allamand, V., Fougerousse, F., Chiannilkulchai, N., Bourg, N., Brenguier, L., Devaud, C., Pasturaud, P., Roudaut, C., and et al. (1995). Mutations in the proteolytic enzyme calpain 3 cause limb-girdle muscular dystrophy type 2A. Cell *81*, 27–40.

Sawyer, S.L., Hartley, T., Dyment, D.A., Beaulieu, C.L., Schwartzentruber, J., Smith, A., Bedford, H.M., Bernard, G., Bernier, F.P., Brais, B., et al. (2016). Utility of whole-exome sequencing for those near the end of the diagnostic odyssey: time to address gaps in care. Clin Genet *89*, 275–284. 10.1111/cge.12654.

Schaffer, A.E., Eggens, V.R., Caglayan, A.O., Reuter, M.S., Scott, E., Coufal, N.G., Silhavy, J.L., Xue, Y., Kayserili, H., Yasuno, K., et al. (2014). *CLP1* founder mutation links tRNA splicing and maturation to cerebellar development and neurodegeneration. Cell *157*, 651–663. 10.1016/j.cell.2014.03.049.

Scott, E.M., Halees, A., Itan, Y., Spencer, E.G., He, Y., Azab, M.A., Gabriel, S.B., Belkadi, A., Boisson, B., Abel, L., et al. (2016). Characterization of Greater Middle Eastern genetic variation for enhanced disease gene discovery. Nat Genet *48*, 1071–1076. 10.1038/ng.3592.

Scott, T.M., Campbell, I.M., Hernandez-Garcia, A., Lalani, S.R., Liu, P., Shaw, C.A., Rosenfeld, J.A., and Scott, D.A. (2021). Clinical exome sequencing data reveal high diagnostic yields for congenital diaphragmatic hernia plus (CDH+) and new phenotypic expansions involving CDH. J Med Genet. 10.1136/jmedgenet-2020-107317.

Seelow, D., Schuelke, M., Hildebrandt, F., and Nurnberg, P. (2009). HomozygosityMapper—an interactive approach to homozygosity mapping. Nucleic Acids Res *37*, W593–599. 10.1093/nar/gkp369.

Smith, C.A.B. (1953). The Detection of Linkage in Human Genetics. Journal of the Royal Statistical Society. Series B (Methodological) *15*, 153–192.

Sobreira, N., Schiettecatte, F., Boehm, C., Valle, D., and Hamosh, A. (2015). New tools for Mendelian disease gene identification: PhenoDB variant analysis module; and GeneMatcher, a web-based tool for linking investigators with an interest in the same gene. Hum Mutat *36*, 425–431. 10.1002/humu.22769.

Spence, J. E., Perciaccante, R. G., Greig, G. M., Willard, H. F., Ledbetter, D. H., Hejtmancik, J. F., Pollack, M. S., OBrien, W. E., and Beaudet, A. L. (1988). Uniparental disomy as a mechanism for human genetic disease. Am J Hum Genet *42*, 217–226.

Szpiech, Z. A., Mak, A. C. Y., White, M. J., Hu, D., Eng, C., Burchard, E. G., and Hernandez, R. D. (2019). Ancestry–Dependent Enrichment of Deleterious Homozygotes in Runs of Homozygosity. Am J Hum Genet *105*, 747–762. 10.1016/j.ajhg.2019.08.011.

Szpiech, Z. A., Xu, J., Pemberton, T. J., Peng, W., Zollner, S., Rosenberg, N. A., and Li, J. Z. (2013). Long runs of homozygosity are enriched for deleterious variation. Am J Hum Genet *93*, 90–102. 10.1016/j.ajhg.2013.05.003.

Tennessen, J. A., Bigham, A. W., OConnor, T. D., Fu, W., Kenny, E. E., Gravel, S., McGee, S., Do, R., Liu, X., Jun, G., et al. (2012). Evolution and functional impact of rare coding variation from deep sequencing of human exomes. Science *337*, 64–69. 10.1126/science.1219240.

Torkamani, A., Pham, P., Libiger, O., Bansal, V., Zhang, G., Scott–Van Zeeland, A. A., Tewhey, R., Topol, E. J., and Schork, N. J. (2012). Clinical implications of human population differences in genome–wide rates of functional genotypes. Front Genet *3*, 211. 10.3389/fgene.2012.00211.

Tuncbilek, E., and Koc, I. (1994). Consanguineous marriage in Turkey and its impact on fertility and mortality. Ann Hum Genet *58*, 321–329.

Wang, K., Li, M., and Hakonarson, H. (2010). ANNOVAR: functional annotation of genetic variants from high–throughput sequencing data. Nucleic Acids Res *38*, e164. 10.1093/nar/gkq603.

Wang, W. Y., Barratt, B. J., Clayton, D. G., and Todd, J. A. (2005). Genome–wide association studies: theoretical and practical concerns. Nat Rev Genet *6*, 109–118. 10.1038/nrg1522.

Wohler E., M. R., Griffith S., Rodrigues E. D. S., Antonescu C., Posey J. E., Coban–Akdemir Z., Jhangian S. N., Doheny K. F., Lupski J. R., Valle D., Hamosh A., Sobreira N. (2021). PhenoDB, GeneMatcher and VariantMatcher,
tools for analysis and sharing of sequence data. *Orphanet J Rare Dis. In press.*

Worthey, E. A., Mayer, A. N., Syverson, G. D., Helbling, D., Bonacci, B. B., Decker, B., Serpe, J. M., Dasu, T., Tschannen, M. R., Veith, R. L., et al. (2011). Making a definitive diagnosis: successful clinical application of whole exome sequencing in a child with intractable inflammatory bowel disease. Genet Med *13*, 255–262. 10.1097/GIM.0b013e3182088158.

Wu, N., Ming, X., Xiao, J., Wu, Z., Chen, X., Shinawi, M., Shen, Y., Yu, G., Liu, J., Xie, H., et al. (2015). *TBX6* null variants and a common hypomorphic allele in congenital scoliosis. N Engl J Med *372*, 341–350. 10.1056/NEJMoa1406829.

Yang, N., Wu, N., Zhang, L., Zhao, Y., Liu, J., Liang, X., Ren, X., Li, W., Chen, W., Dong, S., et al. (2019). *TBX6* compound inheritance leads to congenital vertebral malformations in humans and mice. Hum Mol Genet *28*, 539–547. 10.1093/hmg/ddy358.

Yang, Y., Muzny, D.M., Reid, J.G., Bainbridge, M.N., Willis, A., Ward, P.A., Braxton, A., Beuten, J., Xia, F., Niu, Z., et al. (2013). Clinical whole–exome sequencing for the diagnosis of mendelian disorders. N Engl J Med *369*, 1502–1511. 10.1056/NEJMoa1306555.

Yang, Y., Muzny, D.M., Xia, F., Niu, Z., Person, R., Ding, Y., Ward, P., Braxton, A., Wang, M., Buhay, C., et al. (2014). Molecular findings among patients referred for clinical whole–exome sequencing. JAMA *312*, 1870–1879. 10.1001/jama.2014.14601.

Yengo, L., Wray, N.R., and Visscher, P.M. (2019). Extreme inbreeding in a European ancestry sample from the contemporary UK population. Nat Commun *10*, 3719. 10.1038/s41467–019–11724–6.

Yuan, B., Pehlivan, D., Karaca, E., Patel, N., Charng, W.L., Gambin, T., Gonzaga–Jauregui, C., Sutton, V.R., Yesil, G., Bozdogan, S.T., et al. (2015). Global transcriptional disturbances underlie Cornelia de Lange syndrome and related phenotypes. J Clin Invest *125*, 636–651. 10.1172/JCI77435.

Yuan, B., Schulze, K., Assia Batzir, N., Sinson, J., Dai, H., Zhu, W., Bocanegra, F., Fong, C. T., Holder, J., Nguyen, J., Schaaf, C. P., Yang, Y., Bi, W., Eng, C. M., Shaw, C., Lupski, J. R., & Liu, P. (2021). Sequencing individual genomes with recurrent deletions reveals allelic architecture and disease loci for autosomal recessive traits. Genome Med. *In press*.

Yuan, B., Wang, L., Liu, P., Shaw, C., Dai, H., Cooper, L., Zhu, W., Anderson, S.A., Meng, L., Wang, X., et al. (2020). CNVs cause autosomal recessive genetic diseases with or without involvement of SNV/indels. Genet Med *22*, 1633–1641. 10.1038/s41436–020–0864–8.

Zhang, C., Jolly, A., Shayota, B.J., Mazzeu, J.F., Du, H., Dawood, M., Soper, P.C., Ramalho de Lima, A., Ferreira, B.M., Coban–Akdemir, Z., et al. (2022). Novel pathogenic variants and quantitative phenotypic analyses of Robinow syndrome: WNT signaling perturbation and phenotypic variability. HGG Adv *3*, 100074. 10.1016/j.xhgg.2021.100074.

Zlotogora, J., Gieselmann, V., and Bach, G. (1996). Multiple mutations in a specific gene in a small geographic area: a common phenomenon? Am J Hum Genet *58*, 241–243.

Zollo, M., Ahmed, M., Ferrucci, V., Salpietro, V., Asadzadeh, F., Carotenuto, M., Maroofian, R., Al–Amri, A., Singh, R., Scognamiglio, I., et al. (2017). *PRUNE* is crucial for normal brain development and mutated in microcephaly with neurodevelopmental impairment. Brain *140*, 940–952. 10.1093/brain/awx014.

Figure Legends

Figure 1. **Fine-scale population substructure of TK cohort**

Scatter plots display uniform manifold approximation and projection (UMAP) analysis that compares the population structure among the **A)** TK affected individuals (N=773, colored in purple and dark pink) and **B)** TK unaffected individuals (N=643, colored in dark green and dark orange) of the BHCMG cohort to the African (AFR) (N=661, colored in gray), East Asian (EAS) (N=504, dark blue), European (EUR) (N=503, brown) and South Asian (SAS) (N=489, yellow) population samples from the 1000 Genomes project. **C)** The bar plot demonstrates the results of the admixture analysis performed through the unsupervised ADMIXTURE algorithm (k=5 clusters) quantifying the fraction of ancestry proportions contributed by the African (gray), East Asian (dark blue),

European (brown), South Asian (yellow) and Middle Eastern (pink) for the TK cluster 1 and cluster 2 individuals.

Figure 2. **Comparison of the TK cohort variome to control databases. A)** The Venn Diagram depicts the number of variants present in the TK affected cluster 1 (TKaff-cl1), affected cluster 2 (TKaff-cl2), unaffected cluster 1 (TKunaff-cl1) and unaffected cluster 2 (TKunaff-cl2) individuals (N=3,024,990 variants in total). **B-E)** The pie charts represent all distinct variants in the TK cohorts and whether they are present ('yes') or absent ('no') in gnomAD (upper panel) and the Greater Middle Eastern Variome (lower panel) by affected status and cluster: **B)** unaffected cluster 1; **C)** unaffected cluster 2; **D)** affected cluster 1 and **E)** affected cluster 2.

Figure 3. Higher estimated inbreeding coefficient F values in the TK individuals A) The boxplots report the estimated inbreeding coefficient levels (F) calculated from ES data. Both of the TK affected cluster 1 (purple), affected cluster 2 (dark pink) and unaffected cluster 1 (dark green) and unaffected cluster 2 (dark orange) individuals showed higher F values on average compared to the African (AFR) (gray), East Asian (EAS) (dark blue), European (EUR) (brown) and South Asian (SAS) (yellow) subpopulations from the 1000 Genomes project. **B)** The boxplots show the estimated F values of TK affected cluster 1 (TKaff-cluster1) and cluster 2 (TKaff-cluster2) individuals (mean=0.055 vs. 0.052) were significantly higher compared to the TK unaffected cluster 1 (TKunaff-cluster1) and cluster 2 (TKunaff-cluster2) individuals, respectively (Wilcoxon test one-tailed P-values 2.3e-6 and 2.2e-16). There was no significant difference noted between F values of the TK affected cluster 1 and cluster 2 individuals (P-value=0.34) and the TK unaffected cluster 1 and cluster 2 (P=0.11). P-values indicated above each

pair of groups compared (*<0.05, **<0.01, ***<0.001, ****<0.0001). Outliers are not shown in the boxplots.

C) The scatter plot compares the average fraction of individual genome covered by long-sized (> 2.64 Mb) ROHs (FROH) to the average estimated F values (FIS) for the African (AFR), East Asian (EAS), European (EUR), South Asian (SAS) and TK affected (TK-aff) and TK unaffected (TK-unaff) samples.

Figure 4. **Long-sized ROH regions with increased density of rare deleterious variants are enriched in TK affecteds. A)** The features of long-sized ROHs were displayed irrespective of their total size (Mb) (left panel), the number of ROH blocks (middle panel) and the median length of ROH blocks (Mb) (right panel). In each panel, horizontal boxplots compare the two individual groups as the TK affected (TK-aff) and unaffected (TK-unaff) individuals. A one-sided Wilcoxon rank sum test was used to test the difference in the TK-affected versus TK-unaffected individuals and is indicated to the right of each panel. **B)** We calculated a variant density metric by normalizing the count of rare homozygous deleterious variants to the count of rare homozygous synonymous variants. The density of rare homozygous deleterious variants manifested in long-sized, medium-sized, short-sized ROH regions and not ROH (non-ROH) regions in the TK affecteds (TK-aff) and TK unaffecteds (TK-unaff) subgroups. We then compared the rare homozygous deleterious variant density between the TK-aff and TK-unaff subgroups in each ROH size group and non-ROHs. P-value significance levels were marked on the top of each pair of groups compared (*<0.05, **<0.01, ***<0.001, ****<0.0001). Outliers were not shown in the boxplots.

Figure 5. Contribution of variants in ROH to disease trait phenotype. A) A heatmap depicting the unsupervised hierarchical clustering of the TK affected patients into five general phenotypic categories or groups by calculating a pairwise phenotypic similarity score (clusters 1 (colored in red), 2 (colored in yellow), 3 (colored in green), 4 (colored in blue) and 5 (colored in purple)). **B)** The comparison between the long-sized ROH group to medium-sized, short-sized ROHs and non-ROHs with regard to the performance of their variants in contribution to the disease trait phenotype presented in the TK patients. The y-axis describes the ratios of z-scores calculated for variants located in a specific ROH size group, e.g., long-sized ROH group, versus z-scores calculated for all variants of interest. Z-scores were calculated for each tested disease gene list performing 1,000 simulations. In each simulation, a permuted disease gene list was selected that has a same number of genes as the tested disease gene list. Then, a similarity score was computed between the patient's clinical features and the associated HPO terms of that permuted disease gene list.

Figure 6. **An elevated mutational burden in long-sized ROHs can produce blended phenotypes.**

A retrospective analysis of previously published cases (N=217) compared the cases with diagnoses involving >=2 disease gene loci (N=40) compared to cases with diagnoses involving 1 disease gene locus in terms of **A)** estimated F values, **B)** total span of long-sized ROHs, **C)** deleterious variant density manifested in long-sized ROHs and **D)** total span of medium-sized ROHs.

Supplemental Figure Titles and Legends

Figure S1. Comparison of ancestry component fractions between the TK cluster 1 (N=285) and cluster 2 (N=1,131) individuals. We compared the admixture proportions of the TK cluster 1 and cluster 2 individuals in terms of A) African, B) East Asian, C) European, D) South Asian and E) Middle Eastern ancestry component fractions.

Figure S2. TK variome compared to gnomAD African, East Asian, European and South Asian subpopulation variomes. The pie charts show the comparison of all distinct variants represented in the TK **B)** unaffected cluster 1; **C)** unaffected cluster 2; **D)** affected cluster 1 and **E)** affected cluster 2 to the genome aggregation database (gnomAD) African (AFR) (first panel), East Asian (EAS) (second panel), European (EUR) (third panel) and South Asian (SAS) (bottom panel) subpopulation variome.

Figure S3. Genomic distribution of ROH regions in the TK cohort.

The density of ROH regions present in the TK affecteds and unaffecteds were depicted as a circus plot on each chromosome.

Figure S4. Genomic size features of ROHs detected in the TK cohort.

The features of A) medium-sized, B) short-sized and C) total ROHs were displayed irrespective of their total size (Mb) (left panel), the number of ROH blocks (middle panel) and the median length of ROH blocks (Mb) (right panel). In each panel, horizontal boxplots compare the two individual groups as the TK affected (TK-aff) and unaffected (TK-unaff) individuals. A one-sided Wilcoxon rank sum test was used to test the difference in the TK-affected versus TK-unaffected individuals and is indicated to the right of each panel.

Figure S5. Correlation between total ROH span and the estimated F values in the TK cohort. The scatterplots show the relationship between the estimated F values (y-

axis) and the total length of **A)** long-sized, **B)** medium-sized and **C)** short-sized ROHs (x-axis) for the TK affected (TK-aff) and TK unaffected (TK-unaff) individuals.

Figure S6. The effect of local recombination rate on shaping ROH length in an individual genome. The plot showing that long-sized ROH regions are on average 5.76 times more likely to present with a higher density CS exonic regions vs. HS exonic regions of recombination. These numbers were 4.03, 3.56 and 1.89 for medium-sized, short-sized and non-ROH regions, respectively.

Figure S7. **Total ROH burden among the TK affected and unaffected cluster 1 and 2 individuals.** Boxplots show the total length of ROH segments (Mb) in each size category (**A)** long-sized, **B)** medium-sized, **C)** short-sized and **D)** total ROH in 4 subject groups including the TK affected cluster 1 (TKaff-cluster1) and cluster 2 (TKaff-cluster2) individuals and the TK unaffected cluster 1 (TKunaff-cluster1) and cluster 2 (TKunaff-cluster2) individuals.

Figure S8. **Deleterious variant density among the TK affected and unaffected cluster 1 and 2 individuals.** Boxplots display rare homozygous deleterious variant density manifested in each ROH size category (**A)** long-sized, **B)** medium-sized, **C)** short-sized ROHs and **D)** non-ROHs in 4 subject groups including the TK affected cluster 1 (TKaff-cluster1) and cluster 2 (TKaff-cluster2) individuals and the TK unaffected cluster 1 (TKunaff-cluster1) and cluster 2 (TKunaff-cluster2) individuals.

Figure S9. Correlation between deleterious variant densities in ROHs and estimated F values. The scatterplots show the relationship between the estimated F values (x-axis) and the rare homozygous deleterious variant density presented in **A)**

long-sized, **B)** medium-sized and **C)** short-sized ROHs (y-axis) for the TK affected (TK-aff) and TK unaffected (TK-unaff) individuals.

STAR Methods

CONTACT FOR REAGENT AND RESOURCE SHARING

Requests for further information on raw data, genomic and phenotypic analyses, DNA samples may be directed to, and will be fulfilled by Lead Contact James R. Lupski (jlupski@bcm.edu).

EXPERIMENTAL MODEL AND SUBJECT DETAILS

We recruited 1,416 unrelated TK individuals (669 females and 747 males) in the BHCMG cohort (data freeze: October 2020) After all relevant family members provided written

informed consent for the use of their DNA in identification of disease variants and for broad data sharing. Peripheral blood was collected from affected individuals, parents and unaffected relatives if available. Genomic DNA was extracted from blood leukocytes according to standard procedures. All genomic studies were performed on DNA samples isolated from blood. This study was approved by the Institutional Review Board at Baylor College of Medicine (IRB protocol # H-29697).

MATERIALS AVAILABILITY

This study did not generate unique biological or chemical reagents.

DATA AND CODE AVAILABILITY

All variants reported herein have been aggregated within a TK variome database that is publicly available as a research and molecular diagnostic community resource (https://turkishvariomedb.shinyapps.io/tvdb/). The code generated during this study is available at (https://github.com/BCM-Lupskilab/BafCalculator).

MANDATORY DATA DEPOSITION

Exome variant data have been deposited to dbGaP (study accession phs000711.v5.p1) and/or AnVIL for all cases for which written, informed consent for sharing of data through controlled-access databases has been obtained, in keeping with our IRB and BCM protocol H-29697.

ADDITIONAL METHOD DETAILS

ES and annotation

ES was performed at the Human Genome Sequencing Center (HGSC) at Baylor College of Medicine through the Baylor-Hopkins Center for Mendelian Genomics (BHCMG) initiative. With 1ug of DNA an Illumina paired-end pre-capture library was constructed

according to the manufacturer's protocol (Illumina Multiplexing_SamplePrep_Guide_1005361_D) with modifications as described in the BCM-HGSC Illumina Barcoded Paired-End Capture Library Preparation protocol. Pre-capture libraries were captured into 4-plex library pools and hybridized in solution to the HGSC-designed Core capture reagent (52Mb, NimbleGen) or 6-plex library pools with the custom VCRome 2.1 capture reagent (42Mb, NimbleGen) according to the manufacturer's protocol (NimbleGen SeqCap EZ Exome Library SR User's Guide) with minor revisions. The sequencing run was performed in paired-end mode with the Illumina HiSeq 2000 platform or Illumina NovaSeq 6000 platforms. Data were aligned to GRCh37/hg19 using BWA-aln (for data generated on HiSeq 2000) or BWA-mem (for data generated on NovaSeq). Sequence analysis was performed with the HGSC Mercury analysis pipeline (https://www.hgsc.bcm.edu/software/mercury) (Challis et al., 2012; Reid et al., 2014), which moves data through various analysis tools from the initial sequence generation to annotated variant calls (SNPs and intra-read insertion/deletions; i.e. indels). Variants were called using ATLAS2 or xATLAS (Farek, 2018) and the Sequence Alignment/Map (SAMtools) suites, and annotated with an in-house-developed Cassandra (Bainbridge et al., 2011) annotation pipeline that uses Annotation of Genetic Variants (ANNOVAR) (Wang et al., 2010) and additional tools and databases including ExAC (http://exac.broadinstitute.org), gnomAD (https://gnomad.broadinstitute.org), the GME variome (http://igm.ucsd.edu/gme/), and the ARIC database (http://drupal.cscc.unc.edu/aric/).

Phenotypic characterization of the BHCMG cohort

For this BHCMG project study, we utilized the PhenoDB database to collect and store the information of clinical features, pedigree structures, and self-reported consanguinity levels based on referring physicians' clinical evaluations of research subjects and their unaffected family members. Computational analyses of phenotyping data was performed using HPO terms and essentially as described in (James *et al.*, 2016; Liu *et al.*, 2019b; Posey *et al.*, 2017).

Obtaining a final set of unrelated individuals in the TK cohort

To minimize overrepresentation of individuals from the same family and identify mutually unrelated individuals in the TK cohort, we used the PC-AiR function in the R GENESIS package that measures pairwise kinship coefficients and ancestry divergence to identify an ancestry representative subset of mutually unrelated individuals. Removing individuals with a close relationship from the analysis resulted in a final set of 1,416 unrelated TK individuals: 773 unrelated affecteds and 643 unrelated unaffecteds.

Population substructure analysis

We investigated the population structure of this TK cohort along with the African, East Asian, South Asian and European population samples from the 1000 Genomes Project phase 3 release data including 2,504 individuals' genotypes in total (http://ftp.1000genomes.ebi.ac.uk/vol1/ftp/release/20130502/). First, genotypes for 31 individuals who have a biological relationship with the 2504 samples were removed from the analysis. Variants falling out of the HGSC-designed Core capture design and VCRome 2.1 capture design in the 1000 Genomes Project data were further filtered out from the analysis. A pruned subset of the remaining polymorphic SNVs that is in approximate linkage equilibrium of each other (N=89,379 for the TK affecteds and

N=86,049) was used for the Uniform manifold approximation and projection (UMAP). UMAP was performed using the umap R package. For the admixture analysis, we ran the unsupervised ADMIXTURE algorithm by k=5 clusters that outputted the minimal cross validation error.

Estimation of inbreeding coefficient values

The coefficient of inbreeding of an individual represents the probability that two alleles at any randomly chosen locus in an individual are identical-by-descent.

The inbreeding coefficient values of the TK cohort were estimated from the ES data using plink –het function using only the variants with MAF >= 0.05.

Identifying and analyzing ROH segments from ES data

We detected ROH regions from unphased exome sequence (ES) data as Absence of Heterozygosity (AOH) genomic intervals with BafCalculator (https://github.com/BCM-Lupskilab/BafCalculator) (Karaca et al., 2018). To call ROH regions using BAFCalculator, we extracted all of the high-quality SNVs residing in the capture region (mostly exonic regions) available from the VCF file of each single individual's exome. For those SNVs, we extracted a B-allele frequency (i.e., variant reads/total reads ratio); next, we transformed this ratio by subtracting 0.5 and taking the absolute value for each data point. Transformed B-allele frequency data were then processed using Circular Binary Segmentation (CBS) implemented in the DNAcopy R Bioconductor package (Huber et al., 2015; Olshen et al., 2004) to call the ROH regions. This algorithm merges the consecutive exon calls and so in this way, we can detect ROH regions all over the genome that are of size ranging from hundreds of Kb to a few Mb including a number of genes. To test the false positive and false negative rate of exome data and our algorithm,

BAFCalculator, we ran an independent analysis. We ran the BAFCalculator to call ROH regions from an independent dataset consisting of 929 samples with both genome sequencing (unphased GS) and high resolution phased array data available in the Human Genome Diversity panel (https://www.internationalgenome.org/data-portal/data-collection/hgdp). Then we compared ROH regions identified by the BAFCalculator using the GS data to the ROH regions detected through high resolution array in those 929 samples. Our comparisons showed us that we could further optimize and fine-tune the BAFCalculator algorithm, especially the segmentational mean (seg.mean) parameter (an absolute measure of average homozgosity rate of a putative ROH call). Cross-referencing the ROH regions identified by the fine-tuned BAFCalculator to the array data ROH calls gave us a positive predictive value of 90% and true positive rate of 72% when the seg.mean parameter=0.47 (Supplementary Figure 10). After this analysis, we also took the exome portions of the genome data in those samples and ran the BAFCalculator using only those regions. Then, we compared FROH (the total size of ROHs >= 1.5 Mb) estimates identified from those regions (FROH_WES) to the FROH estimates identified from the whole genome data (FROH_WGS). These analyses also showed us that when the seg.mean=0.47, this gives us nearly perfect correlation (0.98) between FROH_WES and FROH_WGS and WES performs similarly to WGS (Supplementary Figure 11). In summary, segments with the mean signal > 0.47 and number of marks >= 10 were classified as ROH regions. The calculated ROH intervals from BafCalculator could represent individual genomic/gene loci resulting in ROH for diploid alleles that can occur by: i) IBD, ii) UPD (Spence *et al.*, 1988), or iii) a large deletion CNV. To exclude the ROH blocks that could be caused by genomic overlapping of a common variant deletion CNV,

we first identified deletion CNVs through XHMM (Fromer and Purcell, 2014). We further intersected ROH segments and potential deletion CNVs with BEDTools (Quinlan, 2014), and retained only ROH regions overlapping less than 50% of their size with a variant deletion CNV. We grouped ROH regions into three size categories applying Gaussian-mixture modeling using the MClust function in mclust R package unto three length classes: long-sized genomic intervals or ROH blocks (>2.64 Mb), medium-sized ROH blocks (0.671-2.64 Mb), and short ROH blocks (0.210-0.671 Mb).

To control for the variable mutation rates across different genomic regions and among different individuals, for each individual i and ROH region category $r, r \in \{total - ROH, non - ROH, long - sized\ ROH, medium - sized\ ROH, short - sized\ ROH\}$, we computed a variant density $f_{i,r}$

$$f_{i,r} = \frac{N_{i,r}^{d}}{N_{i,r}^{s}}$$

in which $N_{i,r}^{d}$ is the count of rare homozygous deleterious or likely damaging variant alleles (variants above a certain CADD score (>=15) or by utilizing a prediction tool algorithm, NMDescPredictor (Coban-Akdemir *et al.*, 2018)) that are located within a region r, while $N_{i,r}^{s}$ is the count of synonymous variants in a region r.

Generation of an objective score for phenotypic similarity comparison

We applied two R packages, OntologyIndex and ontologySimilarity, to measure the phenotypic similarity between two sets of human phenotype ontology (HPO) terms; each set of terms was associated with a patient's clinical features recorded in PhenoDB (https://phenodb.org/) (Hamosh *et al.*, 2013; Sobreira *et al.*, 2015). To assess the ability

of a disease gene to explain a patient's clinical features, we applied a previously published method, in which first a MICA (most informative common ancestor) matrix was calculated for each pair of HPO terms and then a Resnik score was calculated for two sets of HPO terms (James *et al.*, 2016; Liu *et al.*, 2019b; Posey *et al.*, 2017).

First, we calculated the information content (IC) for HPO term t by

$$IC(t) = -\log(f(t))$$

where $f(t)$ is the frequency of term t observed in all of the OMIM entries. The similarity of term i and term j is calculated with a Resnik method:

$$R_{ij} = IC(MICA(t_i, t_j))$$

where the Resnik score, R_{ij}, is determined by the IC of the most informative common ancestor (MICA) of term i and term j. Next, we defined the phenotypic similarity score Sim for two HPO sets $l_1$and l_2 as follows:

$$l_1 = \{t_{11}, t_{12}, \dots, t_{1m}\}$$

$$l_2 = \{t_{21}, t_{22}, \dots, t_{2n}\}$$

$$Sim(l_1, l_2) = \frac{1}{2}\left(\frac{1}{m}\sum_{i=1}^{m} \max_{1 \le j \le n} R_{ij}, \frac{1}{n}\sum_{j=1}^{n} \max_{1 \le i \le n} R_{ij}\right)$$

The main features of known human disease genes were summarized in OMIM (https://www.omim.org/) in the format of both plain texts and clinical synopses, and the associated HPO terms for each OMIM entry were manually annotated by the HPO-team (https://hpo.jax.org/app/download/annotation). We further adapted this method to measure the phenotypic similarity between a patient's phenotypes and a list of disease genes. For each list of the tested disease genes, we calculated a z-score performing 1,000 simulations; in each simulation we computed a similarity score between the

patient's clinical features and the associated HPO terms of a randomly selected disease gene list, which has a same number of genes as the tested disease gene list. Furthermore, to compare the contribution of disease gene lists across different genomic regions to the explanation of a patient's clinical phenotypic features, we computed a ratio of the similarity score calculated for a subset of disease genes, e.g., genes located in long-sized ROH regions to the similarity score calculated for all of the associated disease genes in a patient's genome.

Statistical Analyses

We performed the statistical analyses with R version 3.3.3. We compared pairwise differences in the average values of estimated inbreeding coefficient values (F), homozygous rare deleterious variant burden (density) and total, median length and count of ROHs in 2 subject groups, TK affecteds and TK unaffecteds using Wilcoxon-rank sum one-tailed test. Bar plots, box plots, pie charts and scatter plots were generated by ggplot2 data visualization R package and stat_pvalue_manual function in the ggpubr R package was used to add P-values and significance levels to those plots. Ddply function in plyr CRAN R package was used to report the summary statistics of estimated F values, homozygous rare deleterious variant burden (density) and total, median length and count of ROHs in 2 subject groups, TK affecteds and TK unaffecteds.

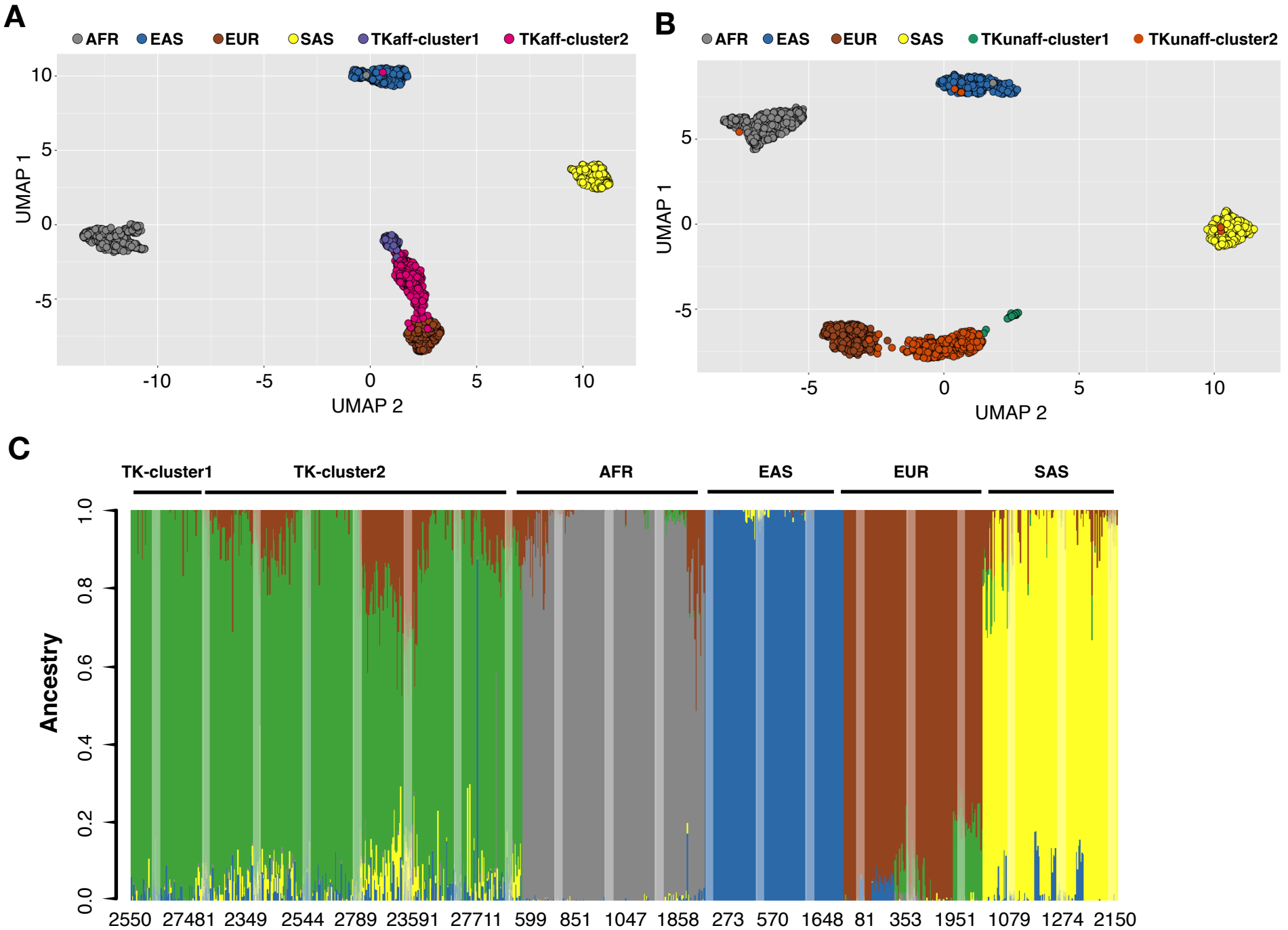
A
AFR
EAS
EUR
SAS
TKaff-cluster1
TKaff-cluster2
UMAP 1
UMAP 2
B
AFR
EAS
EUR
SAS
TKunaff-cluster1
TKunaff-cluster2
UMAP 1
UMAP 2
C
TK-cluster1
TK-cluster2
AFR
EAS
EUR
SAS
Ancestry
2550
27481
2349
2544
2789
23591
27711
599
851
1047
1858
273
570
1648
81
353
1951
1079
1274
2150

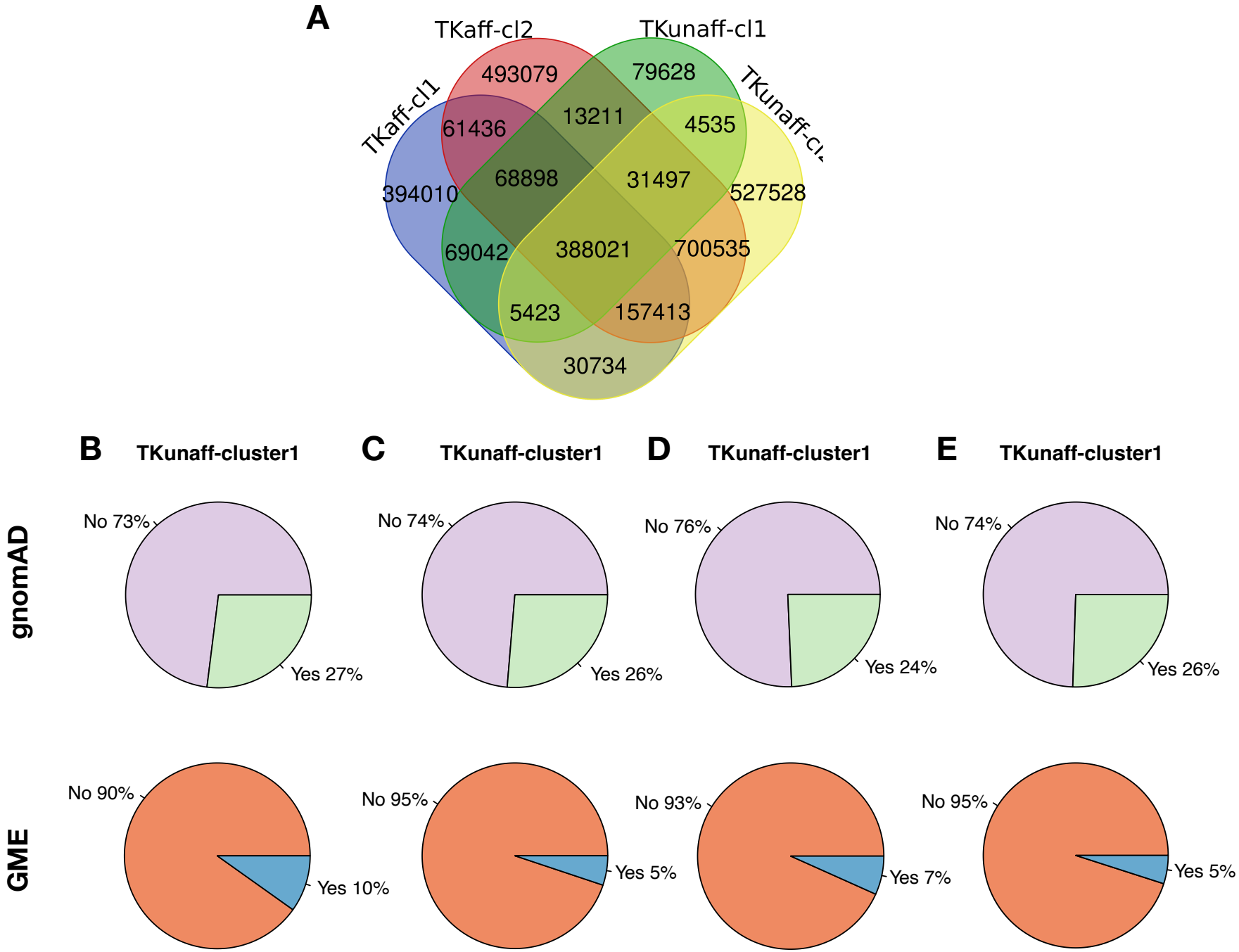
A
TKaff-cl2
TKunaff-cl1
TKaff-cl1
493079
79628
61436
13211
4535
68898
31497
394010
527528
69042
388021
700535
5423
157413
30734
B
TKunaff-cluster1
C
TKunaff-cluster1
D
TKunaff-cluster1
E
TKunaff-cluster1
gnomAD
No 73%
Yes 27%
No 74%
Yes 26%
No 76%
Yes 24%
No 74%
Yes 26%
GME
No 90%
Yes 10%
No 95%
Yes 5%
No 93%
Yes 7%
No 95%
Yes 5%

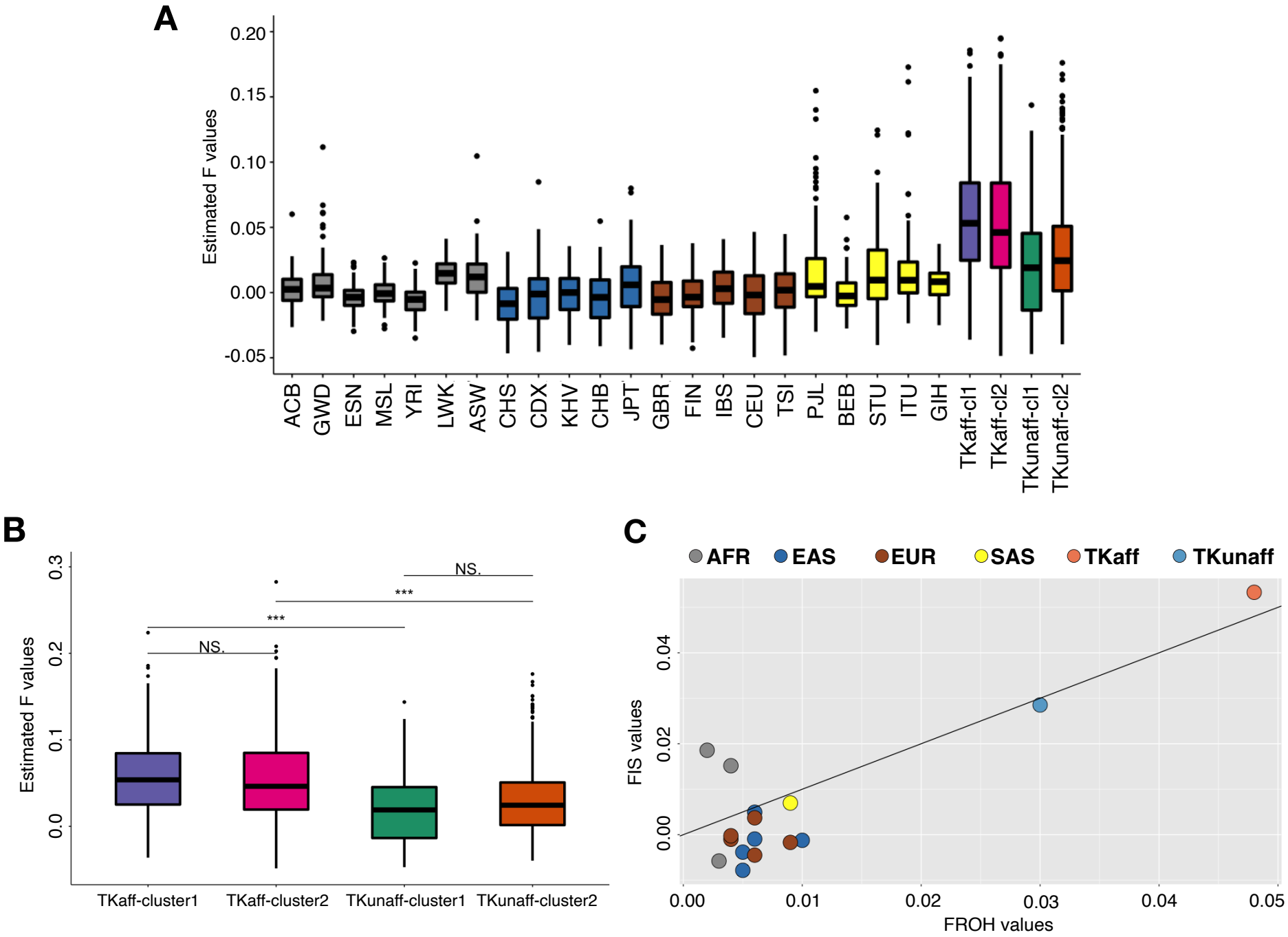
A
Estimated F values
0.20
0.15
0.10
0.05
0.00
-0.05
ACB
GWD
ESN
MSL
YRI
LWK
ASW
CHS
CDX
KHV
CHB
JPT
GBR
FIN
IBS
CEU
TSI
PJL
BEB
STU
ITU
GIH
TKaff-cl1
TKaff-cl2
TKunaff-cl1
TKunaff-cl2
B
Estimated F values
0.3
0.2
0.1
0.0
NS.
***
***
NS.
TKaff-cluster1
TKaff-cluster2
TKunaff-cluster1
TKunaff-cluster2
C
AFR
EAS
EUR
SAS
TKaff
TKunaff
FIS values
0.04
0.02
0.00
0.00
0.01
0.02
0.03
0.04
0.05
FROH values

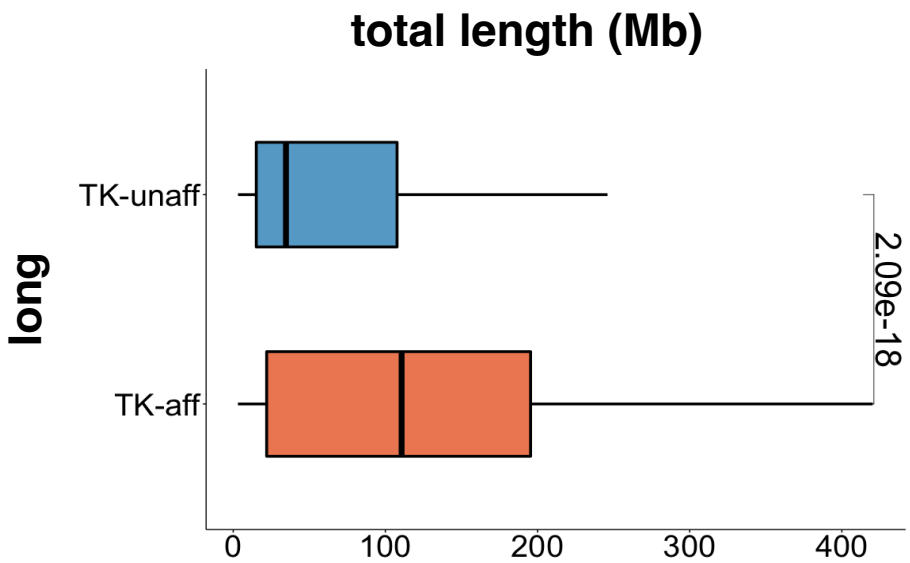
total length (Mb)
long
TK-unaff
TK-aff
2.09e-18
0
100
200
300
400

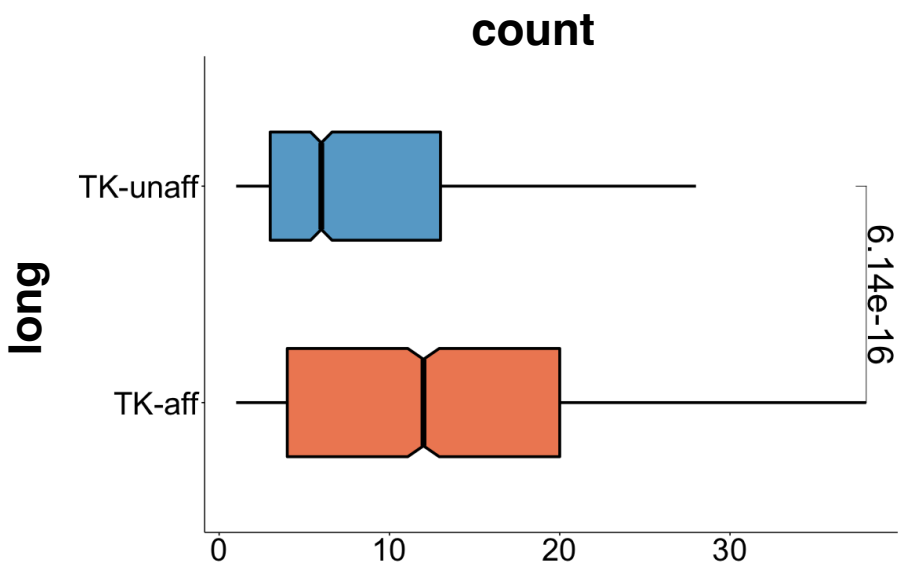
count
long
TK-unaff
TK-aff
6.14e-16
0
10
20
30

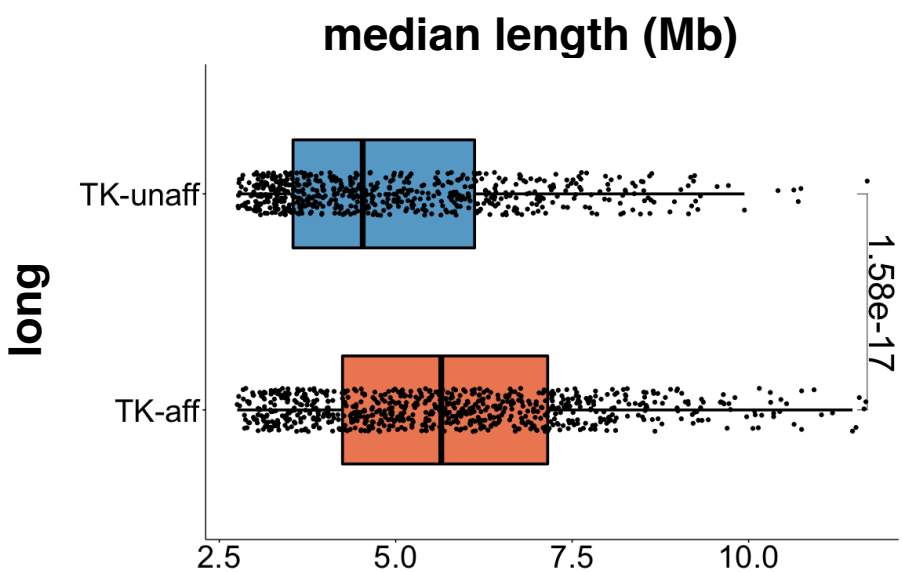
median length (Mb)
long
TK-unaff
TK-aff
1.58e-17
2.5
5.0
7.5
10.0

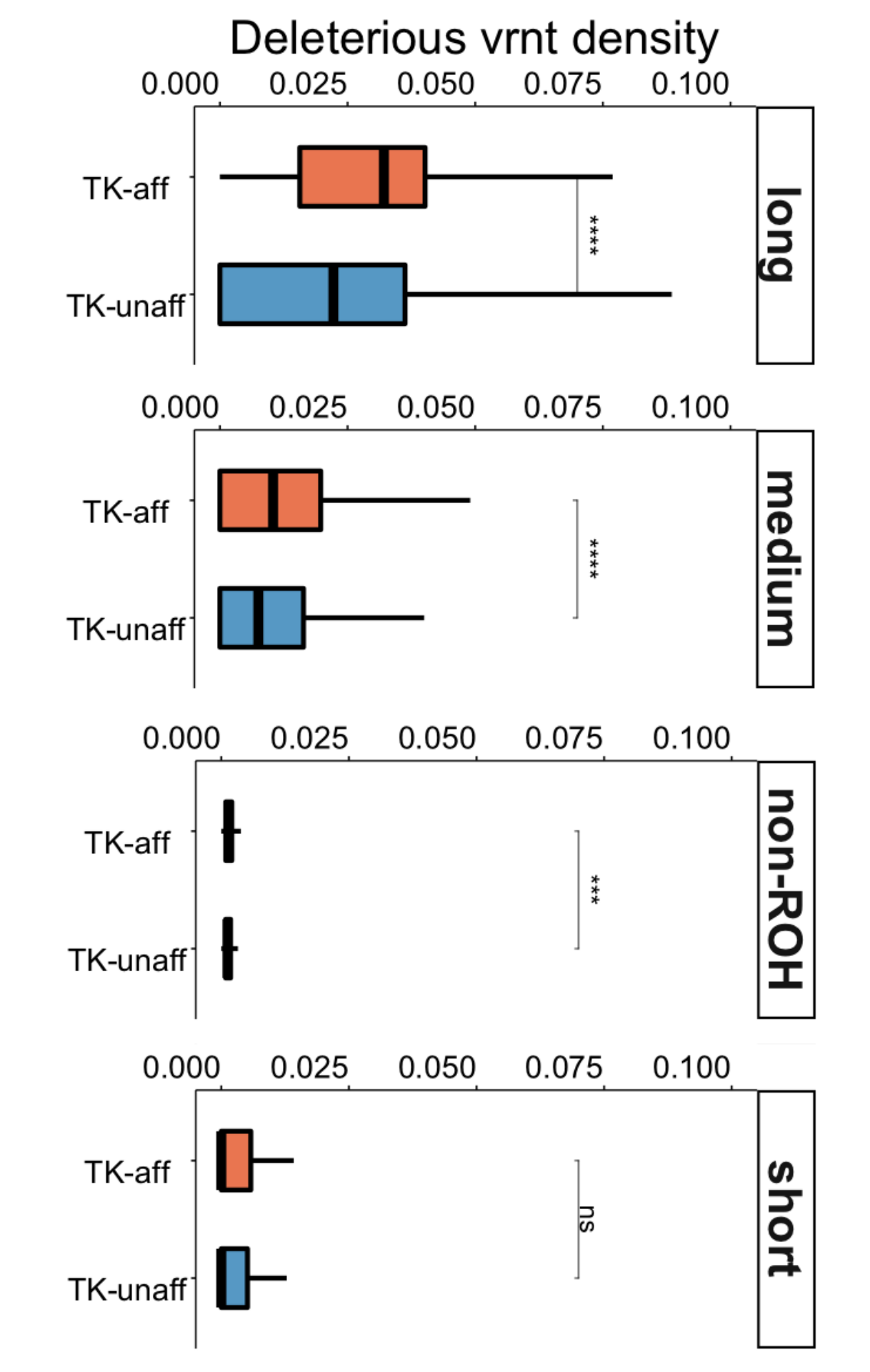
Deleterious vrnt density
0.000
0.025
0.050
0.075
0.100
TK-aff
TK-unaff
****
long
medium
non-ROH
***
short
ns

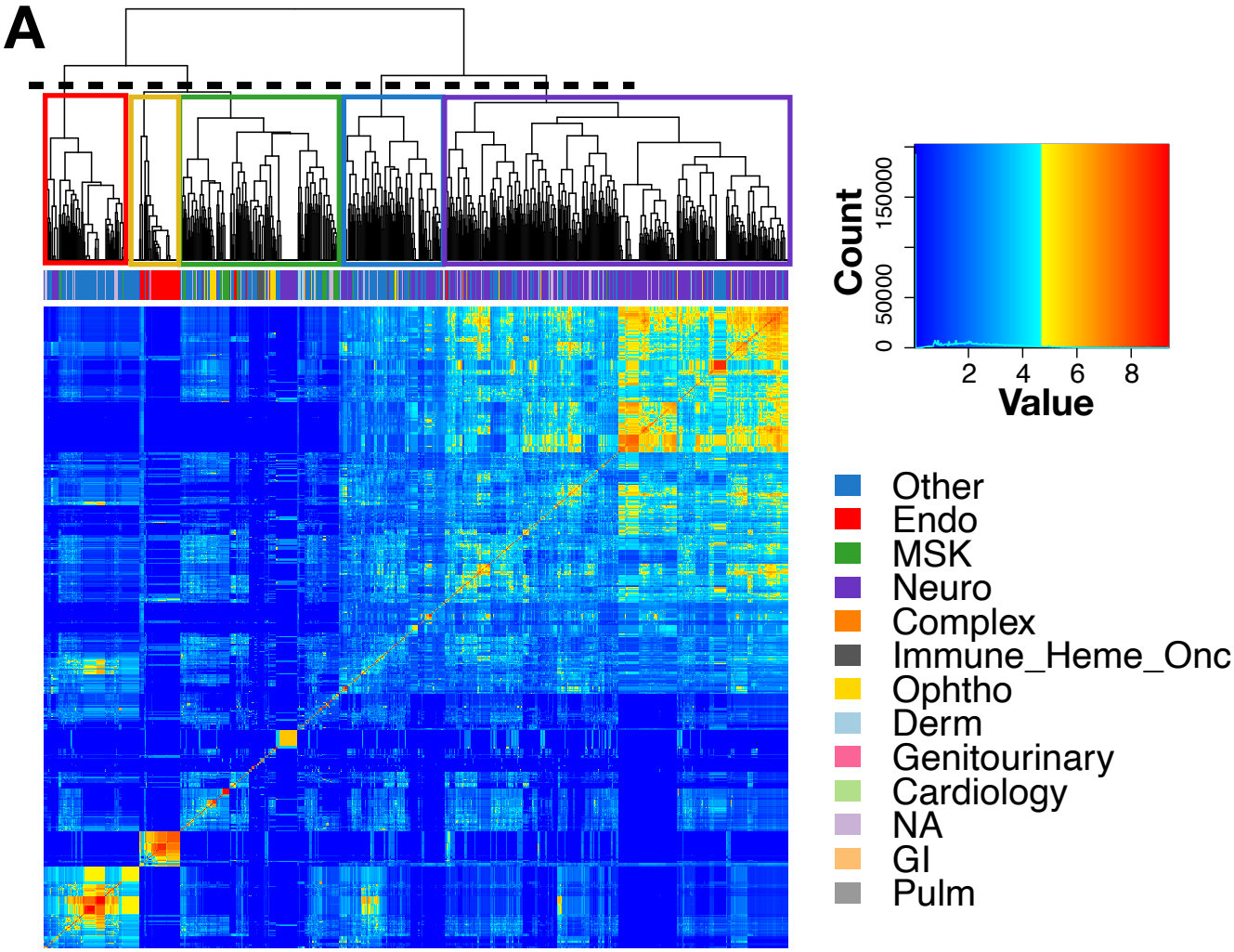
A
Count
0
50000
150000
2
4
6
8
Value
Other
Endo
MSK
Neuro
Complex
Immune_Heme_Onc
Ophtho
Derm
Genitourinary
Cardiology
NA
GI
Pulm

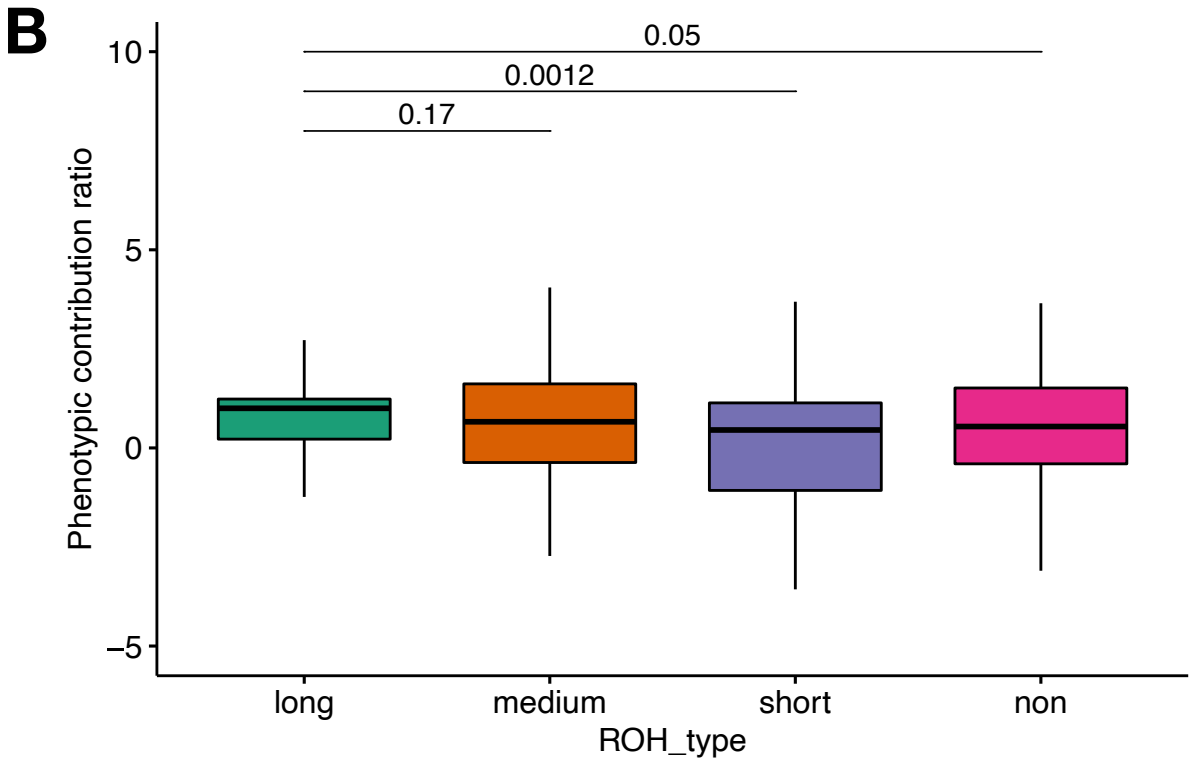
B
0.05
0.0012
0.17
10
5
0
−5
Phenotypic contribution ratio
long
medium
short
non
ROH_type

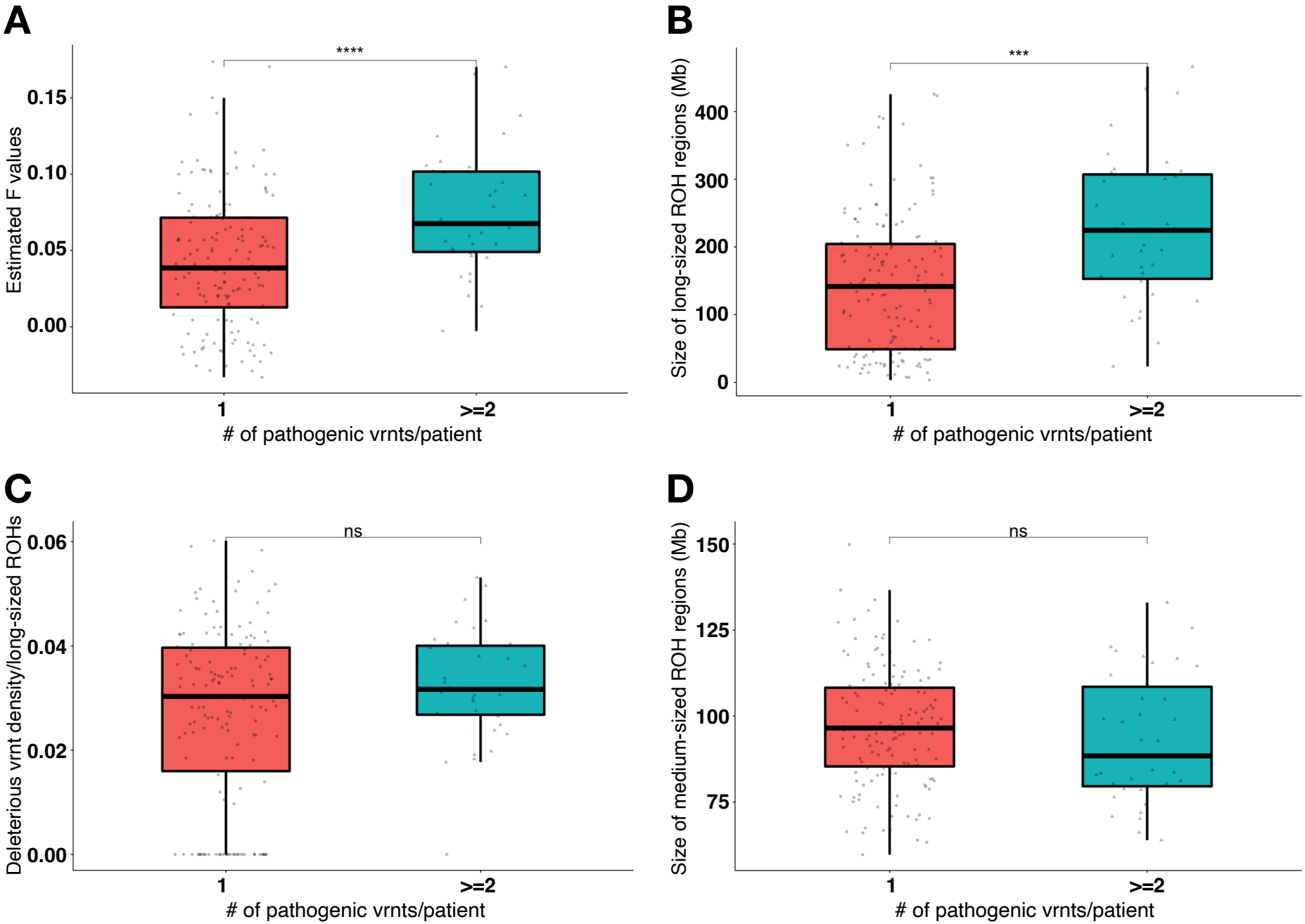
A
****
Estimated F values
0.15
0.10
0.05
0.00
1
>=2
# of pathogenic vrnts/patient
B
***
Size of long-sized ROH regions (Mb)
400
300
200
100
0
1
>=2
# of pathogenic vrnts/patient
C
ns
Deleterious vrnt density/long-sized ROHs
0.06
0.04
0.02
0.00
1
>=2
# of pathogenic vrnts/patient
D
ns
Size of medium-sized ROH regions (Mb)
150
125
100
75
1
>=2
# of pathogenic vrnts/patient